Universidade de Aveiro
Departamento de Electrónica, Telecomunicações e Informática
2018

Fábio Vieira Paulo Henriques

# Performance Analysis of Coherent OFDM-PON in Future Optical Access Networks

# Análise de Desempenho de OFDM-PON Coerente em Futuras Redes de Acesso Óptico

**Fábio Vieira Paulo Henriques**

# Performance Analysis of Coherent OFDM-PON in Future Optical Access Networks

# Análise de Desempenho de OFDM-PON Coerente em Futuras Redes de Acesso Óptico

Dissertação apresentada à Universidade de Aveiro para cumprimento dos requesitos necessários à obtenção do grau de Mestre em Engenharia Eletrónica e Telecomunicações, realizada sob a orientação científica do Prof. Dr. Mário Lima, do Departamento de Eletrónica, Telecomunicações e Informática da Universidade de Aveiro e ao Instituto de Telecomunicações sob Co-orientação científica de Ali Shahpari do Instituto de Telecomunicações.

**o júri / the jury**

presidente / president

**Professor Doutor José Rodrigues Ferreira da Rocha**
Professor Catedrático da Universidade de Aveiro

vogais / examiners committee

**Professor Doutor Mário José Neves de Lima**
Professor Auxiliar da Universidade de Aveiro (orientador)

**Professora Doutora Maria do Carmo Raposo de Medeiros**
Professora Associada da Universidade de Coimbra

**agradecimentos / acknowledgements**

Gostaria de agradecer aos meus pais, avô e tio pelo apoio incondicional prestado durante este meu percurso académico, acreditando sempre no meu sucesso. Sem a sua confiança e força nada disto teria sido possível. Um agradecimento especial ao Tiago Costa, Pedro Santos e Diogo Batista por estarem sempre comigo nesta luta e pelas inúmeras gargalhadas dadas. Não posso deixar, também, de dar um agradecimento especial a todos os amigos e colegas que estiveram presentes nos bons e maus momentos, pois fizeram com que este tempo fosse memorável.

Gostaria também de agradecer ao meu orientador, Professor Doutor Mário Lima, por toda a disponibilidade e ajuda prestada no desenvolvimento desta dissertação.

**Resumo**

A necessidade de aumentar cada vez mais os ritmos de transmissão fazem das comunicações óticas a tecnologia a adotar, sendo esta a única tecnologia que, atualmente, permite transmissão de dados na região dos Tb/s. Todavia, com as redes óticas passivas NG-PON2 é possível obter velocidades de 40 Gb/s downstream e 10 Gb/s upstream mas, devido ao constante aumento de serviços e aplicativos cada vez mais exigentes, é espectável que seja insuficiente para suprimir necessidades futuras, havendo uma incessante investigação de forma a colmatar essas esse défice.

Orthogonal frequency division multiplexing (OFDM) tem vindo a ser utilizado com sucesso em inúmeras aplicações, tais como transmissão áudio/vídeo digital, sistemas de comunicação wireless, entre outras. É uma solução bastante viável que tem a seu favor uma baixa interferência entre símbolos e uma boa eficiência espectral, alem de passar a complexidade dos transmissores e recetores do domínio analógico para o domínio digital.

Nesta dissertação é estudada a tecnologia OFDM, descrevendo todo processo desde geração, modulação, transmissão e receção do sinal. Foi também feito um estudo de simulação exaustivo usando um bit rate de 40 Gb/s e técnicas de modulação avançadas, sendo estas QPSK e 16QAM. Foi também estudado o impacto que as técnicas de deteção direta e coerente têm no sistema, assim como o efeito que o comprimento do canal ótico tem no sinal transmitido.

Esta dissertação visa demonstrar que OFDM é uma tecnologia viável e uma verdadeiras alternativa a ser usada em futuras redes óticas de acesso.

**Abstract**

The need to have ever increasing transmission rates makes optical communications the technology to adopt, being the only technology that currently allows transmission of data in the Tb/s region. However, with passive optical networks NG-PON2 it is possible to achieve speeds of 40 Gb/s downstream and 10 Gb/s upstream but, due to the constant increasing of demanding services and applications, there is an incessant investigation in order to suppress these future needs.

OFDM has been used successfully in numerous applications, such as digital audio/video transmission, wireless communication systems, among others. It is a very viable solution that has in its favor a low interference between symbols and a good spectral efficiency, besides passing the complexity of the transmitters and receivers from analog domain to the digital domain.

This dissertation studies OFDM technology, describing all processes from generation, modulation, transmission and reception of the signal. It is performed an exhaustive simulation study using a 40 Gb/s bit rate and advanced modulation techniques, such as QPSK and 16QAM. It's also studied the impact that direct and coherent detection techniques have on the system, as well as the effect that the optical channel length has on the transmitted signal.

This dissertation aims to demonstrate that OFDM is a viable technology and a true alternative to be used in future optical access networks.

# Contents

# List of Figures

# List of Tables

# Acronyms

| | |
|---|---|
| **ADC** | Analog to Digital Converter |
| **APD** | Avalanche Photodiode |
| **AWG** | Arrayed Waveguide Grating |
| **B2B** | Back to Back |
| **BER** | Bit Error Rate |
| **CO** | Central Office |
| **CW** | Continuous Wave |
| **DAC** | Digital to Analog Converter |
| **DBR** | Distributed Bragg Reflector |
| **CP** | Cycle Prefix |
| **DFT** | Discrete Fourier Transform |
| **DSP** | Digital Signal Processing |
| **EAM** | Electro-absorption Modulator |
| **EDFA** | Erbium Doped Fiber Amplifier |
| **EVM** | Error Vector Magnitude |
| **FDM** | Frequency Division Multiplexing |
| **FEC** | Forward error correction |
| **FFT** | Fast Fourier Transform |
| **FTTH** | fiber-to-the-home |
| **FSAN** | Full Service Access Network |
| **GPON** | Gigabit-Capable Passive Optical Network |
| **ICI** | Inter-Carrier Interference |
| **IDFT** | Inverse Discrete Fourier Transform |

| | |
|---|---|
| **IF** | Intermediate Frequency |
| **IFFT** | Inverse Fast Fourier Transform |
| **IQM** | IQ modulator |
| **ISI** | Intersymbol Interference |
| **LO** | Local Oscillator |
| **MZM** | Mach Zehnder Modulator |
| **NG-PON** | Next Generation Passive Optical Network |
| **OA** | Optical Amplifier |
| **OFDM** | Orthogonal Frequency Division Multiplexing |
| **OFDMA** | Orthogonal Frequency Division Multiplexing Access |
| **OLT** | Optical Line Terminal |
| **ONU** | Optical Network Unit |
| **OSNR** | Optical Signal to Noise Ratio |
| **P2MP** | Point-to-Multipoint |
| **PMD** | Polarization Mode Dispertion |
| **PON** | Passive Optical Network |
| **QAM** | Quadrature Amplitude Modulation |
| **QPSK** | Quadrature Phase Shift Keying |
| **QCSE** | Quantum Confined Stark Effect |
| **RF** | Radio Frequency |
| **SNR** | Signal to Noise Ratio |
| **SSMF** | Standard Single Mode Fiber |
| **TDM** | Time Division Multiplexing |
| **TWDM** | Time Wavelength Division Multiplexing |
| **WDM** | Wavelength Division Multiplexing |
| **XG-PON** | 10 Gigabit-Capable Passive Optical Network |

# Chapter 1

# Introduction

## 1.1 Context and motivation

Communication is nothing more than the transfer of information from point A to point B. With the need to transmit information over long distances, a communication system is required. Within a communication system the information transfer is frequently achieved by superimposing or modulating the information onto an electromagnetic wave which acts as a carrier for the information signal. This modulated carrier is then transmitted to the required destination where it is received and the original information signal is obtained by demodulation [1].

With the evolution of technology and the increase of high-definition multimedia consumption, we need to transfer more and more information at an ever-increasing rate of transmission with high-bandwidth. The commonly used electrical systems do not allow it to do so. These same electrical systems become impractical because, operating in the range of the few hundred Mbit/s, they need regenerators after a few kilometers for the transmission of data. On the other hand, optical systems work in the Gb/s range and only need regenerators after hundreds of kilometers.

Passive optical network (PON) is a promising candidate to meet the bandwidth demand [2]. The first two standards to appear were Ethernet passive optical network (EPON) and Gigabit-Class passive optical network (GPON) and many network operators have started deploying GPON systems to answer the rapidly increasing demand for high bandwidth [3]. However, in order ensure higher data rate, other PON standards have been created, such as the Next Generation passive optical network (NG-PON). There are two types of NG-PON, the NG-PON1 that combines 10 Gigabit-Capable Passive Optical Network (XG-PON) technology with GPON through Wavelenth Division Multiplexing (WDM), and NG-PON2 that had some proposed technologies, among them WDM, Ultra Dense Wavelength Division Multiplexing (UDWDM)-PON, Time Wavelength Division Multiplex (TWDM)-PON and Orthogonal frequency division multiplexing (OFDM)-PON.

Within XG-PON, there is XG-PON1 supporting 10 Gbps downstream and 2.5 Gb/s upstream and XG-PON2 with 10 Gb/s bidirectional on the PON [4]. XG-PON1 has the potential to allow service providers a smooth evolution path for existing residential and business customers served by GPON, by taking advantage of already deployed fiber infrastructure without interfering with the embedded GPON customer base. The XG-PON1 system is designed to be deployed on the same fiber infrastructure as GPON and supports line rates of 10 Gb/s

downstream and 2.5 Gb/s upstream, which is 4 (2) times the downstream (upstream) speed of GPON. [4]. NG-PON2, adopted in 2011 as the following standard, has 40 Gb/s aggregate rate in downstream or upstream. It is a technology that was adopted together with TWDM, taking advantage of the use of multi-channel and tunable wavelenghts [11].

XGS-PON is based on NG-PON2 which was standardized with TWDM-POM to include both asymmetrical 10/2.5 Gb/s and symmetrical 10/10 Gb/s, minus the multi-channel and tunable wavelengths that NG-PON2 offers. The big difference between XG-PON and XGS-PON is that the first only works in 10/2.5 Gb/s asymmetrical mode while the second works in both 10/2.5 Gb/s and 10/10 Gb/s symmetrical. This brings an advantage in which offers new opportunities for operators to monetize their networks more quickly through premium-tier residential services, mobile anyhaul, etc. Another advantage is that CAPEX and OPEX of XG-PON and XGS-PON are quite similar, making it unnecessary to limit options for asymmetric services only [5].

OFDM is a technology that, when applied together with PON, has several advantages such as effective solution to intersymbol interference (ISI) caused by a dispersive channel, transfers the complexity of transmitters and receivers from the analog to the digital domain, among others. The main drawbacks of OFDM are its high peak to average power ratio and its sensitivity to phase noise and frequency offset [6].

This work serves to show that OFDM is a technology to take into account in future access networks due to its ability to transmit high bandwidth and high transmission speeds.

## 1.2 Goals

The main objective of this dissertation is to analyze and demonstrate that OFDM-PON network is a candidate with advantages to take into account for future broadband optical access networks. This dissertation was divided into the following objectives:

- Theoretical analysis of OFDM-PON.
- Simulation analysis of OFDM-PON using direct detection.
- Simulation analysis of OFDM-PON using coherent detection.
- OFDM-PON simulation for different SSMF lenghts and how the lenght influences the system.

## 1.3 Structure

- **Chapter 2: Competing PON Technologies and OFDM-PON architectures**
  This chapter begins with an overview of OFDM's competitive PON technologies. After this phase, a small overview of OFDM will be made, what it is, and all the processes by which it passes to generate electric OFDM. After its generation, it will be explained how the electric signal is converted to the optical domain, the transmition, and then converted back to the electrical domain at the receiver. They will also be explained the different types of receptors, modulators and types of detection that exist.
- **Chapter 3: Simulation**
  This chapter will present the simulations of OFDM setup, through the use of Optiwave's

Optisystem, which allows the simulation and testing of different scenarios using different modulation formats as well as different types of detection and of fiber lenght.

- **Chapter 4: Conclusion and Future Work**
  In this last chapter will be presented the main conclusions obtained from the performed work. It ends with some suggestions for future research.

## 1.4 Main contributions

The main contributions of this work are:

- Demonstrating that OFDM-PON is a relevant technology for future broadband optical access networks, testing it with two different types of detection and two different modulation formats.
- Performance analysis (BER and EVM) of OFDM-PON technology versus both transmitted and received power.

# Chapter 2

# Competing PON Technologies and OFDM-PON architectures

In this chapter, some technologies competing with OFDM will be discussed. PON technologies can be broadly grouped as TDM-PON or WDM-PON. There is still TWDM-PON which is a combination of the two previously mentioned.

PON consists of three main parts: Optical Line Terminal (OLT) which is located at the services provider's central office and provides the interface between PON and the backbone network; Optical Network Unit (ONU), which is located near end users, provide the service interface to end users; Optical Distribution Network (ODN) which, in PON, connects the OLT at the central office and ONUs near user homes by using optical fibers and splitters [7].

## 2.1 Competing PON Technologies

### 2.1.1 TDM-PON

To avoid collision, upstream transmission uses a multiple access protocol (i.e., time-division multiple access) to assign time slots to each user. This type of passive optical network is called TDM-PON[8].

In TDM-PON, the OLT is connected to multiple ONUs through a 1:N passive optical power splitter located near the client. Each output of the splitter is connected to a subscriber. When the OLT sends signals, they are divided into different time slots and each frame contains a frame header for the ONU to be able to identify. These signals are then sent to all ONUs through the 1:N passive optical power splitter. When the signals arrive at the ONUs, each ONU reads the frame header in order to obtain the respective time slot. On the ONU side, the information is sent in burst-mode because all ONUs want to send the information through the same Standard Single Mode Fiber (SSMF). Figure 2.1 ilustrates this architecture.

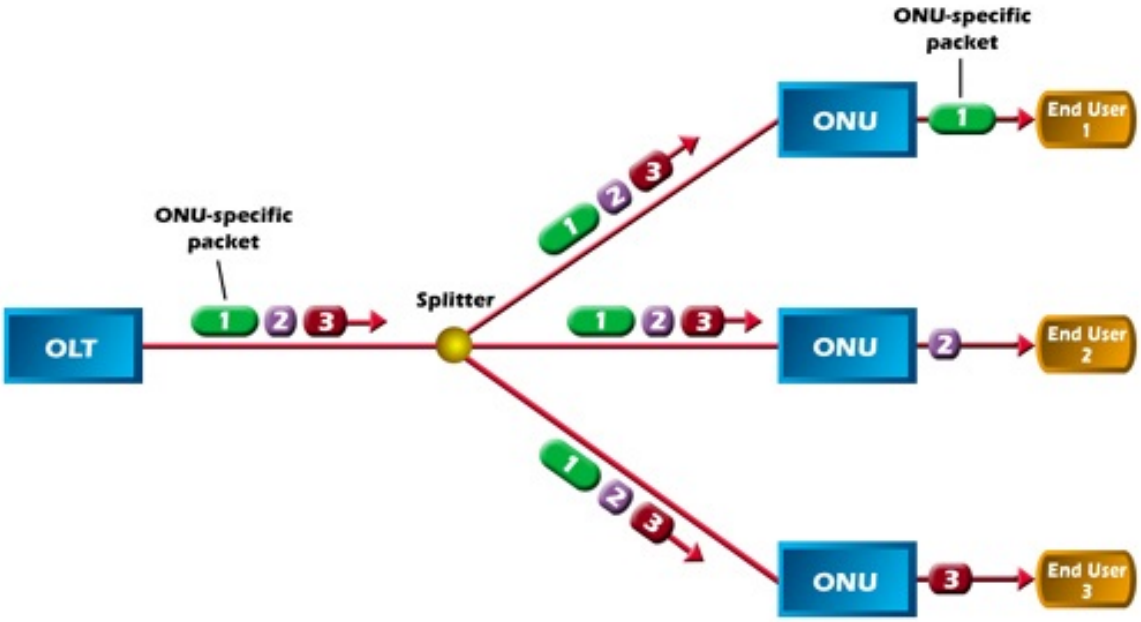


Figure 2.1: TDM PON architecture[9].

The ONU could be located in a home, office, a curbside cabinet, or elsewhere. Thus comes the socalled fiber-to-the-home/office/business/neighborhood/user/premises/node, all of which are commonly referred to as fiber to the x (FTTx) [8].

This type of architecture combines the high capacity given by optical fiber with the low cost of installation and maintenance given by passive infrastructures. The optical carrier is divided by the passive splitter by all subscribers. This leads to the fact that the number of ONUs is quite limited by the attenuation of this same splitter and the working bit rate of the transceivers in the Central Office (CO) and in the ONUs. This is one of the biggest drawbacks of this architecture and makes the current specifications permital for 32 ONUs at a maximum distance of 20 Km from the OLT and 64 ONUs at a maximum distance of 10 Km from the OLT. [10]

### 2.1.2 WDM-PON

The continuous need to increase bandwidth and the limitations presented by TDM-PON, both in the number of ONUs and their distance from the OLT, led to the creation of a new PON, WDM-PON.s

WDM-PON has, as a principle, a separate wavelength channel from the OLT for each ONU, for each of the upstream and downstream directions. In the illustration given by figure 2.2, it is based on a point-to-point (P2P) link between the CO and each ONU, which differs from the point-to-multipoint (P2MP) topology of the regular PON (TDM-PON). With this, each ONU can operate at a rate up to the full bit rate of a wavelenght channel. This system has capability to provide each client different services using the same network, through WDM-PON that allows telecommunication providers to use different sets of wavelengths to support different independent PON subnetworks, all operating over the same fiber infrastructure [10].

In the figure 2.2 it is possible to observe that on the left side we have the OLT side, where

the CO resides, and on the right side we have the ONUs side. There is an array of transmitters and receivers on each side. Each transmitter-receiver pair in the OLT and ONU works with a specific wavelength that connects to a multiplexing device. In this configuration, a arrayed waveguide grating (AWG) is used as a multiplexer or demultiplexer. The AWG is a passive optical device with the special property of periodicity, which is the cyclic nature by which multiple spectral orders are routed to the same output port from an input port. This allows for spatial reuse of the wavelength channels [10].

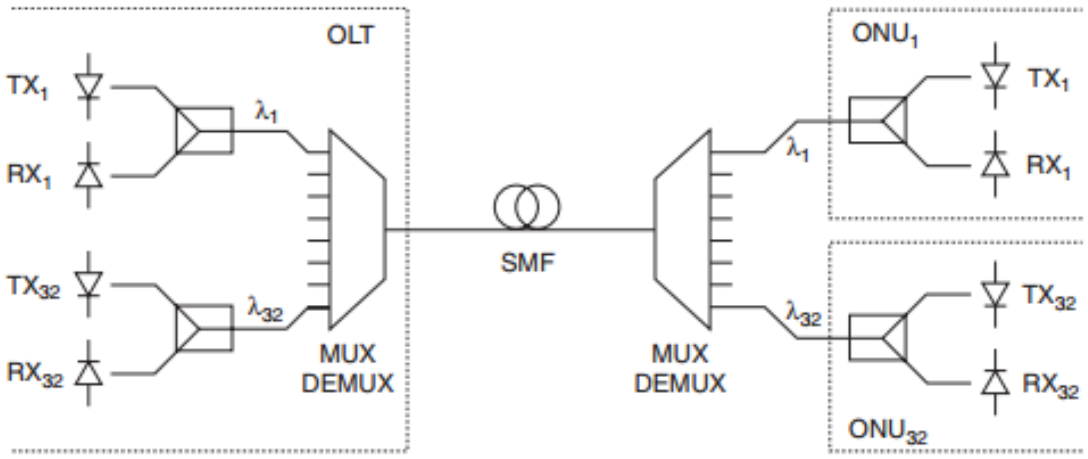


Figure 2.2: WDM PON architecture[8].

On the downstream direction, the system sends a multiwavelength channel from the OLT to multiple ONUs through a multiplexer device (in this case AWG). It's used SSMF to connect the OLT to the AWG, between the two AWGs, as well as to connect the second AWG to the ONUs. On the upstream direction the OLT employs a WDM demultiplexer and a receiver array for receiving the upstream signals. It is to be noted that each ONU has a transmitter and receiver to transmit and receive in its respective wavelength [10].

In order to avoid an inventory problem, we need to take into account certain aspects, such as the need to all ONUs transmitters and receivers to be colorless, that is, wavelenght independent, so that all devices used on the client side are all the same. If the ONUs are not colorless, the service provider would have to have many different types of ONUs in stock for replacement and would have to customise each ONU for each customer, which would carry additional costs [10].

Another approach to take into account to solve the inventory problem is the tunable light sources, as they provide flexibility and reconfigurability for network provisioning, which minimizes production costs and reduces the backup stock required [8]. Yet, although they solve the inventory problem, these do not receive much attention because tunable sources have been developed for use in long-haul or metro-core networks and their cost is too high for the network access applications [10].

### 2.1.3 TWDM-PON

The NG-PON2 project was started by the Full Service Access Network (FSAN) community in 2011. It investigates on optical fiber network technologies enabling a bandwidth increase beyond 10 Gb/s in the access network.

There are some requirements that must be met by new technologies in order to be adopted as solution for NG-PON2. Some major requirements are at least 40 Gb/s aggregate rate in downstream or upstream, 40 km reach, 1:64 split ratio, 40 km differential reach, and at least 1 Gb/s access rate per ONU [11].

Many PON technologies have been proposed to provide broadband optical access beyond 10 Gb/s [12], among them WDM-PON, OFDM-PON which apply quadrature amplitude modulation and fast Fourier transform to generate digital OFDM signals for transmission [13], Optical Code Division Multiplexing Access PON (OCDMA-PON) and also TWDM-PON.

Within all the proposals presented, TWDM-PON attracted the greatest support by the community and, in 2012, was selected by FSAN as the preferred solution for NG-PON2. The reasons for selecting TWDM-PON for NG-PON2 are the large split ratio offered, which helps in achieving lower cost and power consumption per user, it inherently supports the high flexibility of resource allocation, which allows it to efficiently adapt to the varied traffic demands from the end user [14].

To increase the capacity of a single feeder fiber in NG-PON2, leveraging WDM technologies is necessary. This is done by stacking multiple XG-PON1 subsystems in the wavelength domain. A XG-PON1 system offers the access rates of 10 Gb/s in downstream and 2.5 Gb/s in upstream. They are accredit individual optical channels between two wavebands for channels upstream and downstream [11] [14]. Therefore, a TWDM-PON system with 4 pairs of wavelenghts is capable of providing 40 Gb/s downstream and 10 Gb/s upstream. Each TWDM-PON ONU can give peak rates up to 10 Gb/s downstream and 2.5 Gb/s upstream, which makes it meet the imposed requirements [11].

Coexisting with previous PON generations is one of the main wavelenght contrains for TWDM-PON and, in order to solve this problem, there are several options. One option is to reuse existing XG-PON1 wavelenght bands, defining a finer grid of this bands. The idea behind this wavelenght plan is to reuse and take advantage of the development work that has been done on XG-PON1. This option is compatible with GPON and radio frequency (RF) video overlay, but blocks standardized XG-PON. Another option is to use the C-band to contain both upstream and downstream wavelength. This is an option that allows the use of Erbium Doped Fiber Amplifier (EDFA) to amplify the signal and thus makes the transmission distances longer with low transmission losses. This wavelenght plane is compatible with both GPON and XG-PON1 but RF video overlay channel is blocked. There is still one more option, which is a mixture of the two plans previously presented where the downstream channels are located in the L-plus band and the upstream channels are located in the C-minus band. This wavelenght plan is compatible with both GPON and RF video overlay but blocks XG-PON1. This option uses the EDFA to amplify the signal in the downstream direction and pre-amplify in the upstream direction [11].

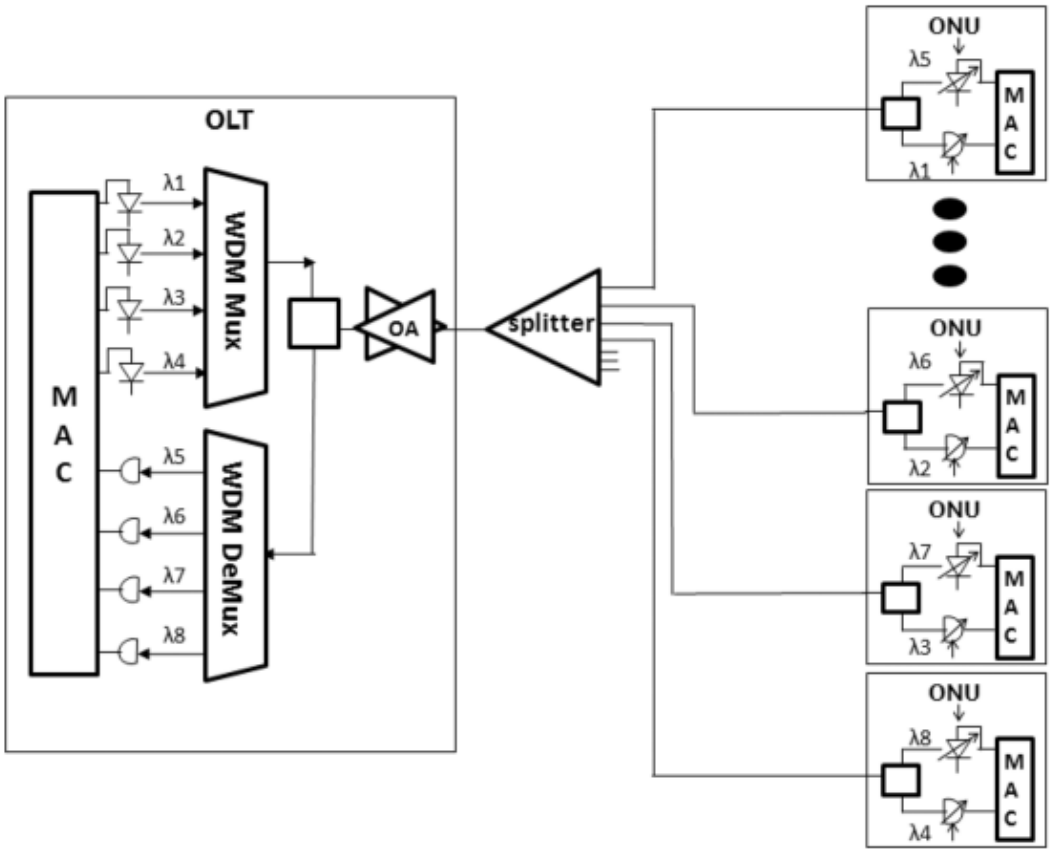


Figure 2.3: TWDM PON architecture[11].

In the figure 2.3 we can see an example of a typical TWDM-PON architecture. Four XG-PON1s are stacked by four pairs of wavelenghts. On the OLT side, each wavelength of 10 Gb/s is multiplexed, thus prefiguring the 40 Gb/s and sent in the direction downstream, passing by optical amplifiers (OA). These OAs are used both to boost the downstream signal, as to pre-amplify the upstream signals. The signal then passes through a splitter whose function is to distribute power to all the ONUs, causing all ONUs to receive signals from all wavelenghts. A tunable filter is used on the receiver to select or tune to any of the four downstream wavelenghts. In the case of the upstream wavelenghts, a tunable laser is used of way to provide colorless ONU, thus promoting the reduction of costs of implementation and maintenance of the network.

NG-PON2 operates with upstream transmitters in burst mode over 4 X 100 GHz or 8 X 50 GHz channels around 1530 nm. Burst lengths range from $0.5\mu s$ to $125\mu s$, with a $125\mu s$ periodicity, where laser bias current is turned off between bursts and turned on during bursts [15].

One of the problems inherent in TWDM-PON is that laser becomes self-heating and couses a wavelength red-shift at the beginning of each burst. This causes strong power variations in the receiver and leads to a significant reduction in sensitivity. A proposal presented recently to combat this problem is based on a Distributed Bragg Laser Reflector (DBR), where there is a compensation of the deviation by applying a small signal to the Bragg section, stabilizing

the frequency in a few nanoseconds. This DBR sollution has excelent results for TWDM-PON, however, it is required refined control to ensure the correct operation of the system and stable operation [15].

There has also been research into making TWDM-PON more energy-efficient. In these systems, the only active components responsible for energy consumption are OLT and ONUs. The absense of upstream data, especially in low load, creates many idle periods (also known as voids) between two consecutive transmissions of upstream data at OLT receivers. These voids promote an opportunity to design more energy efficient OLT receivers for these systems. Recently, there were some proposals where the main principle is to use only a few wavelengths for scheduling. These wavelengths are called active wavelengths. The remaining wavelengths are designated as inactive and are those that have the OLT receiver off. The main goal of these proposals is to minimize the number of active wavelengths in order to maximize energy efficiency [16].

## 2.2 OFDM-PON

OFDM is currently one of the most efficient and reliable solution for high-rate transmission in optical communications [17] and has emerged as a dominant R&D area in the field of high-speed optical communications [18].

Regarding next-generation optical access, there are two aspects to consider that favor OFDM, being the first access network "capacity crunch" driven by digital video traffic, mobile backhaul, in-home networking, etc.[19], and the second related to a P2MP network topology that is unique to this fiber-optic application domain [18] [20]. Clearly, with the prediction of a large number of global FTTH deployments increase based on P2MP PON and with the expected increase of subscribers, it is evident that the PON architectures will play a key role in future access networks. Furthermore, for the next generation access technology, both on the wireless network and on the PON network, the bandwith resources are shared between several users. A technique that has been widely adopted, takes advantage of the OFDM signal and has been applied in wireless networks is known as Orthogonal Frequency Division Multiple Access (OFDMA)[18]. This technology has a unique advantage for future PON systems, more specifically in the highly bursty traffic profile in PON, combined with a drive towards multi-service coexistence on a single platform, would make flexible, transparent inter user and/or service bandwidth sharing a premium [20].

In figure 2.4 is presented a illustration of a single-wavelenght OFDMA-PON architecture. In this architecture, for downstream transmission of heterogeneous services, the frequency and time domain of an OFDMA frame is performed by the OLT, with the resulting time/frequency broadcast to all of the ONUs over non-reserved OFDM subcarriers and pre-configured time slots [18][21]. This OFDMA frame then passes through the SSMF, a 1:N splitter and arrives on the receiver. On the receiver side, each ONU has a digital signal processing (DSP), which is used to recover its pre-assigned OFDM subcarriers and/or time slots. For the upstream direction, each ONU maps its data to a designated OFDM subcarrier, nulls all remaining subcarriers and performs OFDM modulation in order to build a complete frame. This frame then passes through a coupler that injects this frame created by the ONU in the SSMF towards the OLT. By supporting a variety of services and data rates, the heterogeneous ONUs in an OFDMA-PON can thus help achieve a high network flexibility and effectively manage cost[18].

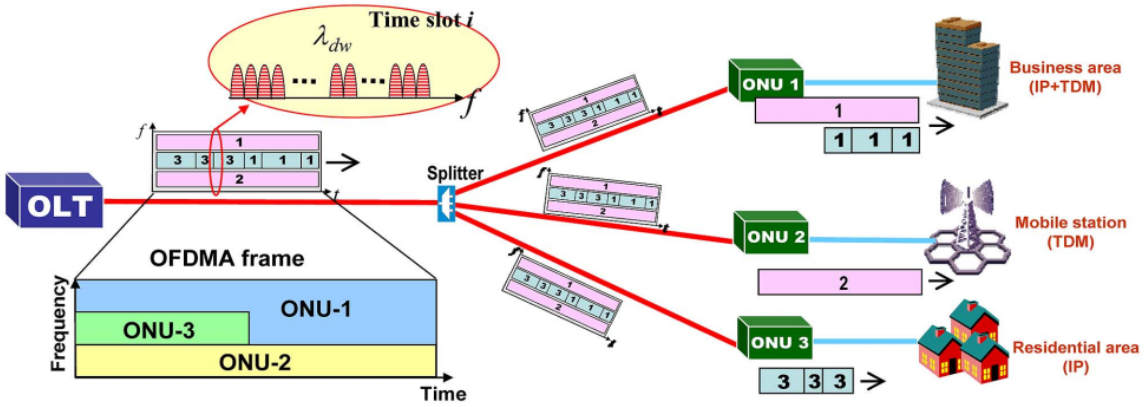


Figure 2.4: OFDMA PON architecture for delivery of heterogeneous services with single-wavelength upstream transmission[18].

Different OFDM subcarriers will be located to different ONUs, furthermore, each OFDM subcarrier can also be shared to 2-D multiuser bandwidth partitioning, as we can see in figure 2.4. In addition, the properties of this technique allow it to combine one and 2-D bandwidth provisioning. Analyzing figure 2.4 and, for example, while ONU-2 keeps a fixed subcarrier assignment for several frames, ONU-1 and ONU-3 fit together in time-domain and share the same OFDM subcarrier. Since traffic is aggregated and disaggregated electronically, this technique can propagate over existing architecture, which translates into cost savings. In order for OFDM subcarriers to be recovered by the DSP, this technique requires a accurate synchronization to allow multiuser access for both downstream and upstream direction[18].

## 2.3 OFDM Overview

In a classical parallel data system, the total bandwidth of the signal can be divided in N non-overlapping frequency subchannels in which each subchannel is modeled for a different symbol, and then the N subchannels are modeled in frequency. One of the major purposes of avoiding spectral overlap of subcarriers is to eliminate inter-carrier interference (ICI)[22].

Frequency division multiplexing (FDM) divides the total data rate to be sent by several subcarriers. This data does not necessarily have to come from the same source of information nor does it have to be divided equally by the subcarriers [23]. The main advantage of using this technique is the possibility to use modulation/demodulation personalized to a exact type of data, or transmitting out banks of dissimilar data that can be best sent using multiple, and possibly different, modulation schemes. However, FDM systems usually need to use a guard band between subcarriers to prevent the spectrum of a subcarrier from overlapping with others subcarriers' spectrum. This represents a major disadvantage in terms of spectral efficiency. In figure 2.5 is shown an illustration of a FDM transmission.

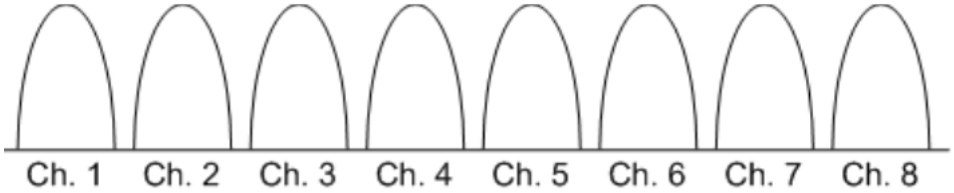


Figure 2.5: FDM channels separated by guard bits[22].

The principle behind OFDM is to take advantage of the spectrum that FDM wastes, rearranging the subchannels in order to overlap the sidebands of the individual carriers without causing ICI. This is only achievable due to the orthogonality between the subchannels possible by the Fourier transform, so the guard band previously needed to ensure the demodulation of the subcarriers on the FDM systems will no longer be required. As long as the orthogonality of the system is maintained, it is possible to recover the individual subcarriers' signals despite its spectrum being overlapped.

The transmitted multi-carrier signal s(t) is given by:

$$s(t) = \sum_{i=-\infty}^{+\infty} \sum_{K=1}^{N_{sc}} c_{k,i} \cdot e^{j2\pi f_k t} \cdot P(t - iT_s) \tag{2.1}$$

where $N_{sc}$ is the number of subcarriers, $c_{k,i}$ is the ith information OFDM symbol at the kth subcarrier, $f_k$ is the subcarrier frequency, $P(t)$ is the pulse shaping function and $T_s$ is the duration of each OFDM symbol[24]. $f_k$ must satisfy the orthogonality condition:

$$f_k = k \cdot \frac{1}{T_s} \tag{2.2}$$

where K is the number of subcarriers. Each subcarrier is separated by $\frac{1}{T_s}$ [24]. The amplitude spectrum of the OFDM signal is given by a $sinc(\pi ft)$, where all frequencies $f_k$ are multiple by $\frac{1}{T_s}$.

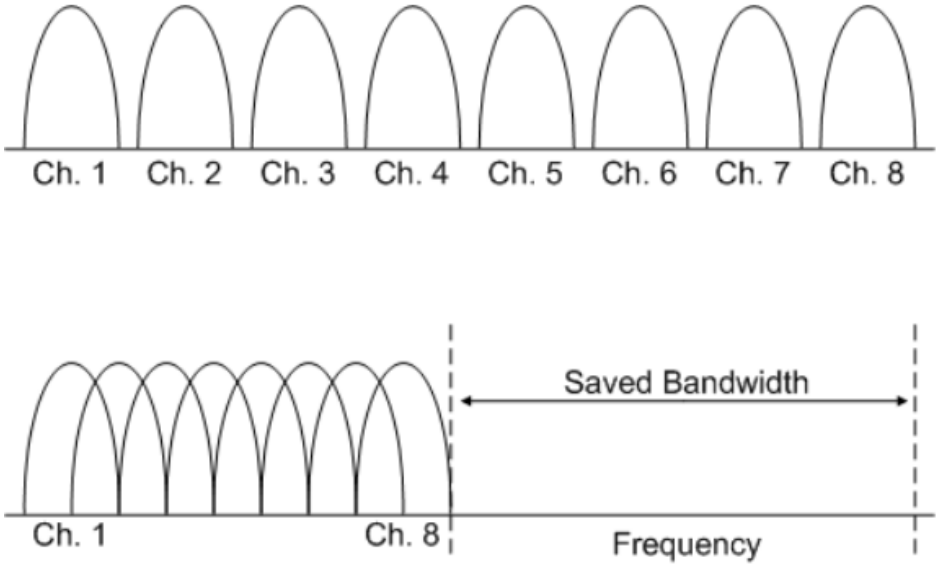


Figure 2.6: FDM versus OFDM frequency spectrum of eight channels (a) FDM techniques (b) OFDM techniques[22].

In figure 2.6 we see a comparison of the spectral frequency of an FDM signal comparatively with an OFDM signal. From the analysis, we see that the bandwidth used by the OFDM signal to transmit the same data is reduced by about 50%. This shows a much higher efficiency than the FDM signal because it allows the sub-channels to overlap to the adjacent channels.

## 2.4 Electrical OFDM

In figure 2.7 is presented the typical block diagram with the different stages both for the generation and trasmition of an OFDM signal and for the reception of an OFDM signal.

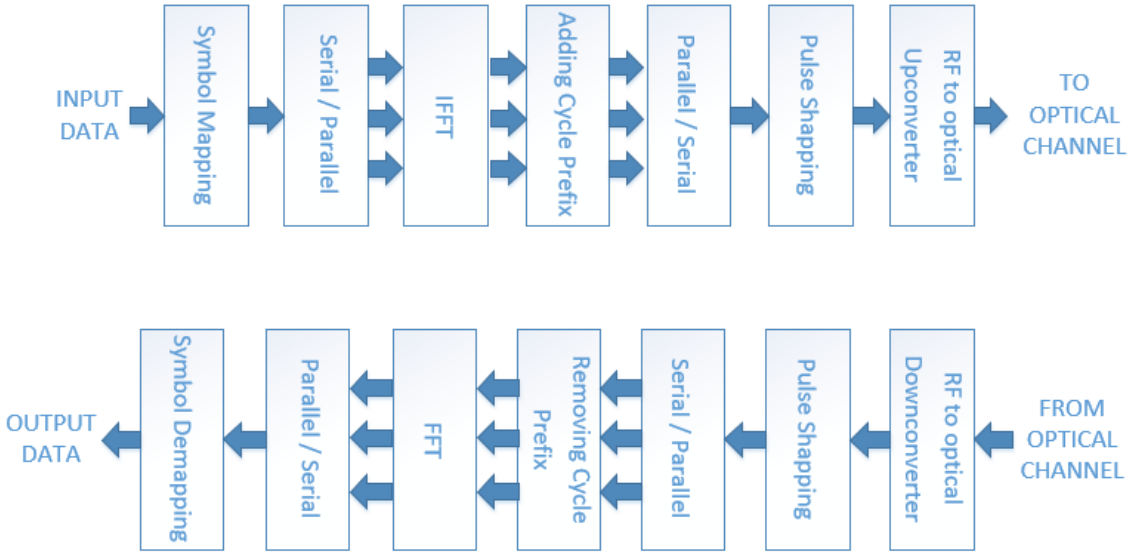


Figure 2.7: Block diagram of a typical OFDM transmitter and receiver

### 2.4.1 Symbol Mapping and Demapping

At this stage, after the first stage where a random bit sequence is generated, it is where the bit mapping in order to have a number of symbols per subcarrier. Here a complex modulation format is used, such as M-Quadrature Amplitude Modulation (QAM) or any of its variants, or Quadrature Phase Shift Keying (QPSK). Taking the QPSK modeling as example, two input bits are used to generate each of the four complex symbols, as shown in figure 2.8. It is possible for the system to have more bits per symbol in higher order systems, as is the case of 16QAM that uses 4 bits per symbol.

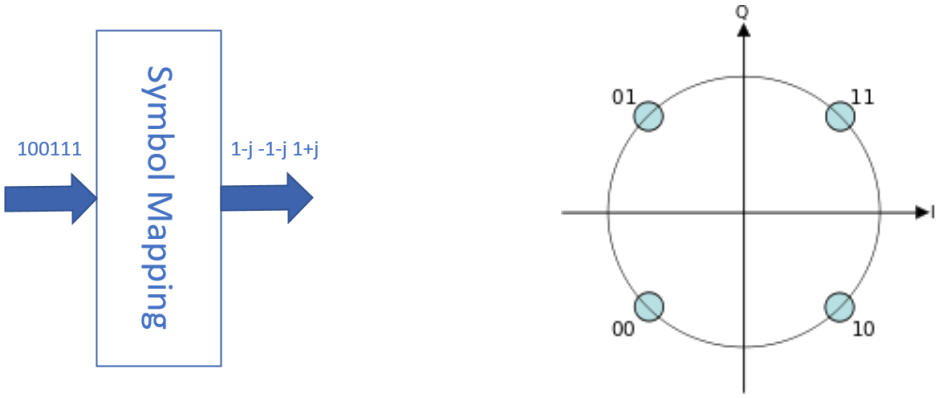


(a) (b)

Figure 2.8: QPSK mapping

On the receiver side, each incoming symbol will be demapped in order to obtain the bit stream originally transmitted. In figure 2.9 we have an example of the received constellation and the demapping of the symbols from complex symbols to real symbols. One of the existing problems is the fact that transmission lines always have dispersion and other types of imperfections. These always insert some kind of error into the transmitted signal. In this way and as it is possible to see in figure 2.9a, the constellation in the receiver will be distorted thus requiring a decision threshold in order to know which constellation point corresponds each distorted point. This decision threshold has to be made before the demapping of the symbol.

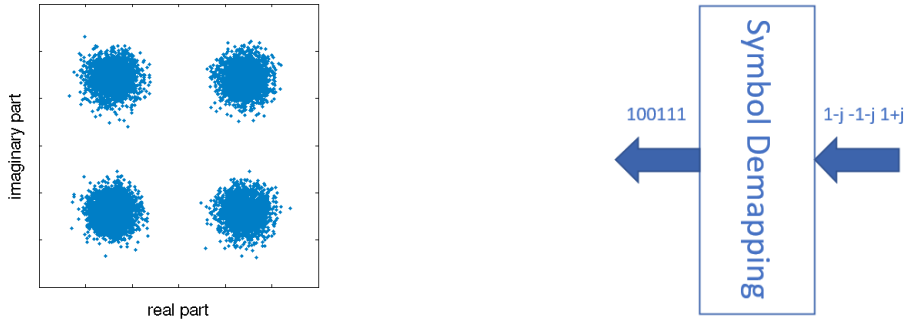


(a) (b)

Figure 2.9: QPSK demapping.

### 2.4.2 Serial to Parallel Conversion and Parallel to Serial Conversion

On the transmitter side, the modulated input serial data stream is injected into the block and transformed from serial to parallel, this means the data will be converted from serial high speed input to a low speed parallel output signal. Every low speed signal that leaves the block corresponds to a subcarrier output, as shown in figure 2.10a. On the receiver side, the inverse operation occurs, where arrives low speed parellel signals in the input and in the output we will have high speed serial signals, represented in figure 2.10b


(a) (b)

Figure 2.10: (a) Serial to Parallel convertion and (b) Parallel to Serial convertion.

### 2.4.3 IFFT and FFT

The Inverse Fast Fourier Transform (IFFT) and Fast Fourier Transform (FFT) blocks are the most important in an OFDM system, in the transmitter and receiver, respectively. These are the functions that distinguish OFDM from single carrier systems [6]. These blocks are mathematically equivalent versions of Discrete Fourier Transform (DFT) and Inverse Discrete Fourier Transform (IDFT), respectively, but more efficient to implement in practice. These mathematical operations are vastly used to transform data between time-domain and frequency-domain. To perform these operations, the IFFT matches the frequency-domain data input with its orthogonal basis functions, which, at certain frequencies, are sinusoids. This is the equivalent of mapping the input data onto the sinusoidal basis functions [23].

Nevertheless, to create an OFDM signal with a large number of subcarriers, we will have an extremely complex architecture, both on the transmitter and receiver side. To observe this, on the next equation, we will only take into account one symbol of 2.1 and assume that we sample s(t) at every interval of $\frac{T_s}{N}$.

$$s(\frac{nT_s}{N}) = \sum_{N-1}^{k=0} c_k e^{j2\pi f_k \frac{nT_s}{N}} = \sum_{N-1}^{k=0} c_k e^{j2\pi \frac{kn}{N}} = \mathcal{F}^{-1}\{c_k\} \tag{2.3}$$

where the $\mathcal{F}$ is the Fourier transform and n $\in$ [1,N].
On the receptor side, we will have

$$c'_k = \mathcal{F}\{r_m\} \tag{2.4}$$

where $r_m$ is the received signal sampled at every interval of $\frac{T_s}{N}$. The OFDM signal transmitted s(t) is a simple N-point IDFT of the information symbol $c_k$ and a received information symbol $c'_k$ is a simple N-point DFT of the received sampled signal [24].

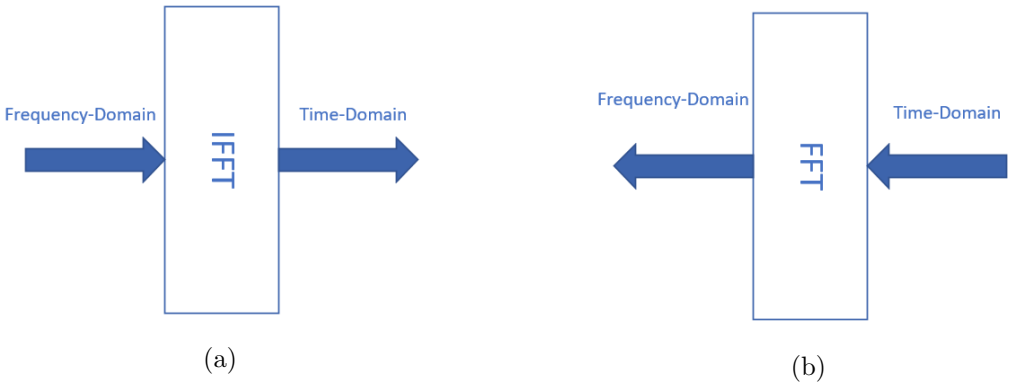


(a) (b)

Figure 2.11: (a) IFFT block that transforms signal from frequency-domain into time-domain and (b) FFT block that transforms signal from time-domain into frequency-domain.

On the IFFT, each input symbol is complex as it comes from the mapping block, which will determine both the amplitude and the sinusoidal phase of the subcarrier. On the IFFT output we will have a sum of all N sinusoidal that makes up for a single OFDM symbol with a NT size, where T is the IFFT input symbol period. After some additional processes, the output of the IFFT block is transmitted by the transmission channel and reaches the receiver. On the receiver, after passing through the removal of the CP and still in time-domain, the signal goes by the FFT, where it is processed and transformed back to the frequency-domain. Ideally, the FFT output will be equal to the the IFFT input on the transmitter [23].

### 2.4.4 Cyclic prefix

The Cycle Prefix (CP) block, also referred to as a cycle extension or guard interval, is one of the most important blocks that allow the OFDM technique. Firstly, the subcarriers are aligned in the transmitter side but, when transmitted by a channel with dispersion, some symbols suffer a bigger delay than other symbols. This causes the slower subcarriers to cross the symbol boundary leading to interference between neighboring OFDM symbols, resulting on the so-called ISI. In addition, due to the loss of orthogonality of the system, this results in ICI[24].

CP is on the insertion of some predefined tail-end portion of an OFDM date frame to its beginning, causing the frame to begin and end the same way, hence the "cyclic" quality. Since the size of the CP at least the same size as the delay caused by dispersion, there is no longer any ISI because the portion that would be overlapped by the next subcarrier will be absorbed by the CP instead of the front-end data symbols. Therefore, and seen from this perspective, the only characteristic that matters is the size of the CP and not its content. In the short, the CP can be an asset to other situations, as it turns the channel's time-domain dispersive effect from a linear convolution into a cyclic convolution such that no matter how long the impulse response becomes, as long as the CP is as long, data symbols can still be recovered via single-tap equalization in the frequency domain. As correlation technique, CP can be used to determine the beginning and end of each data frame, which is key to align the receiver-side FFT window and thus avoid ISI and ICI [18].

In figure 2.12 is shown an example of two OFDM symbols transmitted one after the other and how they are affected by the dispersion of the transmission channel.

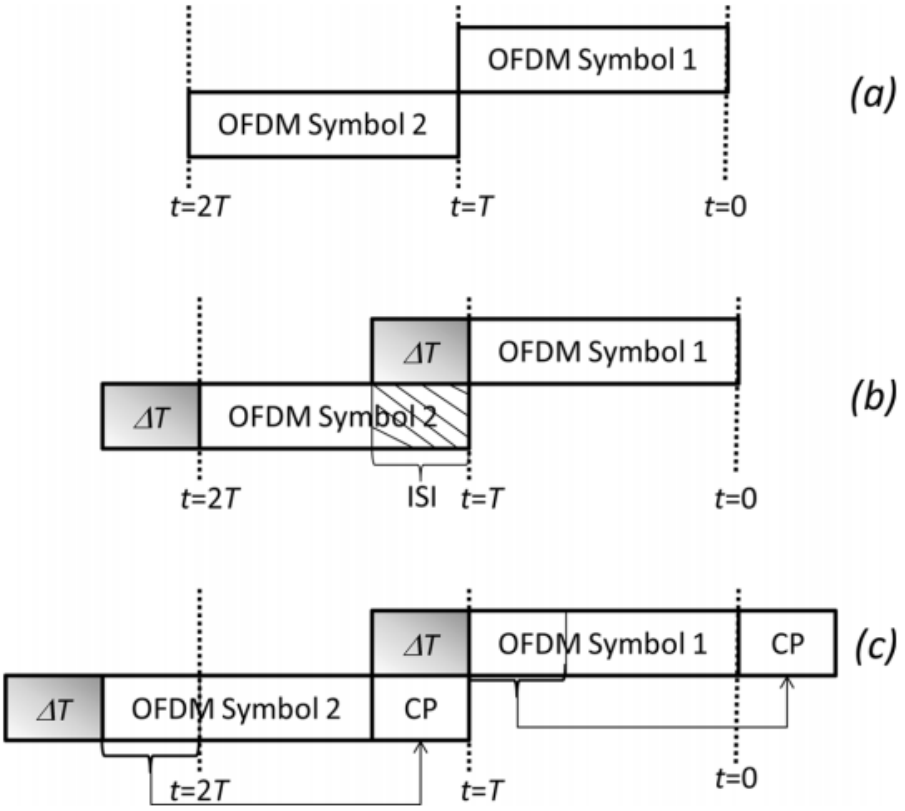


Figure 2.12: OFDM symbol transmission in (a) ideal, nondispersive channel, (b) dispersive channel without CP insertion, resulting in ISI, and (c) dispersive channel with CP insertion used to eliminate IS[18]

In figure 2.12a we have two OFDM symbols without CP transmitted in an ideal nondispersive channel, which is unrealistic in real world applications because the smaller sample timing error, relatively small frquency synchronization or phase noise results in ICI. In figure 2.12b we have the overlap of Symbol 1 with Symbol 2, thus resulting ISI. This is avoided by using

CP, as shown in figure 2.12c, where the end of each symbol is copied to its beginning, causing the portion that would be superimposed to be contained in the CP, thereby eliminating ISI.

A disadvantage of this principle is a slight loss of effective transmit power, since we are inserting a guard interval that is redundant in the transmission. Usually, the size of the guard interval is between one tenth to one quarter of the symbol period, leading to an SNR loss of 0.5 to 1 dB [25].

### 2.4.5 D/A and A/D conversion

In the transmission and after the conversion from parallel to serial, the signal must pass through a digital to analog to convert (DAC). The DAC is used to convert the transmitted signal from discrete to a continuous value. On the receiver side, an analog to digital converter (ADC) is used. The ADC is used to do the inverse operation, convert the analog signal received to a continuous value.

### 2.4.6 Pulse Shapping

OFDM systems are quite sensitive to frequency offset that leads to the appearance of ICI and performance degradation [26].One technique to combat this phenomenon is through the use of pulse-shaping filters [27], where root raised cosine pulses have been proposed and are widely adopted for transmitter and receiver filters [28]. In this block, the signal is filtered by a pulse-shaping filter and has to satisfy the Nyquist ISI criterion.

The raised-cosine pulse (in the time domain) is given by

$$p_{rc}(t) = \begin{cases} \frac{1}{T} & 0 \leq |t| \leq \frac{T(1-\alpha)}{2} \\ \frac{1}{2T}\left\{1 + \cos\left[\frac{\pi}{\alpha T}\left(|t| - \frac{T-\alpha}{2}\right)\right]\right\} & \frac{T(1-\alpha)}{2} \leq |t| \leq \frac{T(1+\alpha)}{2} \\ 0 & otherwise \end{cases} \tag{2.5}$$

in which the Fourir transform is $P_{rc}(f)$ and where $\alpha$ is the roll-off factor and $0 \leq \alpha \leq 1$. $\alpha$ controls how sharply the pulse spectrum is. When $\alpha = 0$, the raised-cosine pulse coalesce into a rectangular pulse [26].

### 2.4.7 RF to optical upconversion and RF to optical downconverter

After the generation of a RF-OFDM signal, there is a need to convert it from the electrical domain to the optical domain before transmitting it over the transmission channel. For this, the signal has to go through the RF to optical converter block.

In figure 2.13a we have a coherent optical OFDM system that uses direct up/down conversion arquitecture and, in figure 2.13b, a system which uses intermediate frequency (IF) architecture. In the direct up/down conversion architecture (figure 2.13a), the baseband OFDM signal $S_B$ (for one OFDM frame) can be written as

$$S_B(t) = \sum_{k=-(N_{sc}/2)+1}^{k=N_{sc}/2} C_k e^{j2\pi f_k t} \qquad , f_k = (k-1)/t_s \tag{2.6}$$

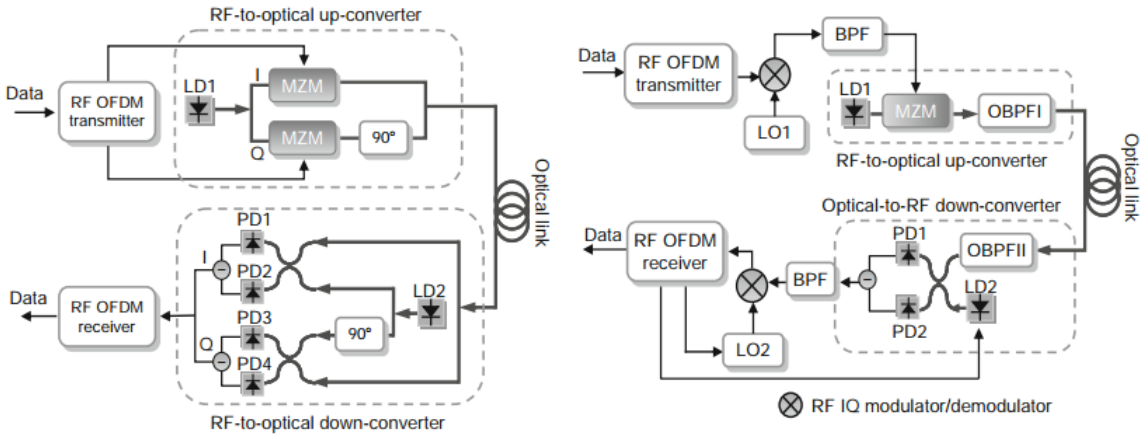


Figure 2.13: CO-OFDM system with (a) direct up/down conversion architecture and (b) IF architecture [24]

---

where $N_{sc}$ is the number of subcarriers, $t_s$ is the OFDM symbol period, $C_k$ is the $k_{th}$ subcarrier, and $f_k$ is the frequency of the subcarrier [29].

An optical I/Q modulator is used in the optical transmitter consisting of two Mach-Zehnder Modulators (MZMs) to up-convert the real and imaginary part of the complex OFDM signal from RF domain to optical domain, one of the MZM with the real part and the other with the imaginary part of the signal $S_B(t)$. In the direct down-converter arquitecture (on the receiver side), the OFDM optical receiver uses two pairs of balanced receivers and an optical 90 degree hybrid in order to do optical I/Q detection. The RF OFDM receiver performs OFDM baseband processing and demodulation to recover the data [24]. This architecture eliminates the need for narrow optical bandpass filters on the transmitter and receiver [29].

In the IF architecture (figure 2.13b), the the OFDM IF signal after the RF modulator can be written as

$$S_{IF}(t) = e^{j2\pi f_{LO1} t} \cdot \sum_{k=1-N_{sc}/2}^{k=N_{sc}/2} C_k e^{j2\pi f_k t} \qquad , f_k = (k-1)/t_s \tag{2.7}$$

In the IF up-conversion architecture, the signal goes through two steps. First, the OFDM baseband signal is up-converted to an intermediate frequency $f_{LO1}$, still in the electric domain, and then up-converted once more to the optical domain with the use of one MZM. In IF down-conversion, the optical OFDM signal is down-converted to an intermediate frequency $f_{LO2}$ and, subsequently, the electrical I/Q detection is done [24].

## 2.5 Optical OFDM

### 2.5.1 Optical OFDM Transmitter

In this section will be shown different types of modulations typically implemented in optical systems.

One of the main functionalities of optical systems is modulation, which consists of "converting" the high bit-rate electrical data signal into the optical domain. Ideally, this process subsists on the translation of the frequency from the baseband to an optical carrier frequency, of the order of 193 THz for the ususal 1550nm transmission window [30].

Most optical communication systems use intensity modulation of the lightwave, where its intensity or power is varied according to the data to be transmitted. This allows for a simpler detection process where a photodiode is used which generates a photocurrent proportional to the incoming optical power [30].

#### 2.5.1.1 Direct Modulation Systems

Direct modulation uses a digital modulation current on the top of the current bias. This bias current is chosen so that the logical levels of modulation current, which correspond to bits 0 and 1, are above the laser threshold current [31]. The power in the output of a laser semiconductor is dependent on the current injected through the laser diode, where the transfer function is represented by figure 2.14.

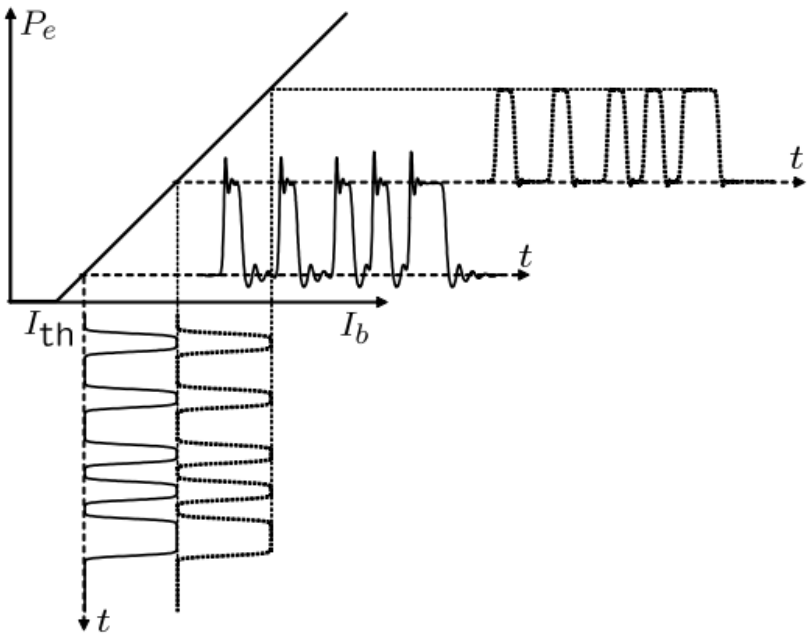


Figure 2.14: Ilustration of the concept of direct current modulation of a semiconductor laser [30]

Until the current reaches the threshold value $I_{th}$, the diode will not emit light (except spontaneous emission). After the threshold, population inversion is achieved, leading to the

function of the laser. The power generated by the laser grows linearly with increasing current, until a bias current is too high and the laser becomes saturated [30].

In spite of its simplicity and being possible to use for high speed (up to 40Gb/s in certain lasers but mostly used up to 10 Gb/s), this modulation technique is not commonly used due to problems such as frequency chirp, nonuniform frequency response, and large current swing needed to provide operation [32].

The transmission distance is characterized by the point at which the signal degradation, called Bit Error Rate (BER), exceeds a certain value. BER is mostly caused by chromatic dispersion, which scales proportionally with the laser frequency chirp and dispersion properties of the optical fiber [31]

#### 2.5.1.2 External Modulation Systems

Another form of modulation is through an external process that occurs after the generation of light. Here, a laser diode produces a Continuous Wave (CW), which will be the input of the external modulator. In the modulator, a digital modulation voltage is used to change between the logic levels. Despite the increase in complexity in comparation to the direct modulation technique, the external modulation has great advantages, such as the increase of both the modulation bit rate and the transmission distance [31]. This happens because the optical pulses are nearly chirp-free [33].

Some of the most used are Electro-absorption Modulator (EAM), Mach-Zehnder Modulator (MZ) and IQ Modulator (IQM).

- **Electro-absorption Modulators :** EAM is an appealing solution for applications that require high speed modulation, low drive voltage, high extinction ratio and integrability with lasers [34].

  EAM are based on the electroabsorption effect, which is the change of material absoption in the presence of an electric field [35]. In bulk materials, this process is known as Franz-Keldysh effect, whereas in quantum-well materials it is called the Quantum Confined Stark Effect (QCSE). The main difference between this two types of materials is the model for absorption. In the first and due to the absorption of a photon, an electron is raised from the valence band for the conduction band maintaining the same momentum and, despite the energy changing according to each vertical transition, the force of all transitions is considered equal. In the second, only transitions between states of the same quantum number, both in the valence band and conduction band, are allowed and momentum may not be saved.

  Figure 2.15 shows an illustration of the Franz-Keldysh effect. When a high electric field E is applied to a semiconductor, tilting in the energy bands is achieved and results in enhanced electron tunneling between the valence and conduction bands (represented by $E_v$ and $E_c$ in figure 2.15, respectively) thereby increasing the absorption, also for photon energies below $E_g$[36].

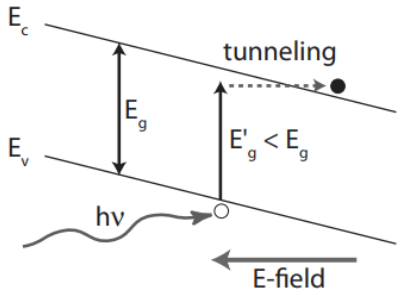


Figure 2.15: Illustration of Franz-Keldysh effect[36]

Equation 2.8 describes the effective shift of the bandgap

$$\Delta E_g = -\frac{3}{2}\left(\frac{q\hbar E}{\sqrt{m^*}}\right)^{2/3} \tag{2.8}$$

where q represents the electron charge, $\hbar$ represents Planck's constant divided by $2\pi$ and $m^*$ is the electron effective mass [kg].

For QCSE, the absorption edge is much sharper and moves faster with reverse biased electric field, making this devices favorable in achieving a low drive voltage, low insertion loss and high extinction ratio [35]. Figure 2.16 shows an illustration of QCSE. As the field increases, the overlap of electron and holes waveforms is reduced, decreasing both the absorption strength and the transition energy. On the other hand, the formation of electron-hole pairs (excitons) improves the absorption. Comparing thick and thin quantum wells, we can verify that the first offers advantageous field sensitivity (high modulation efficiency) while the second gives strong absorption [34].

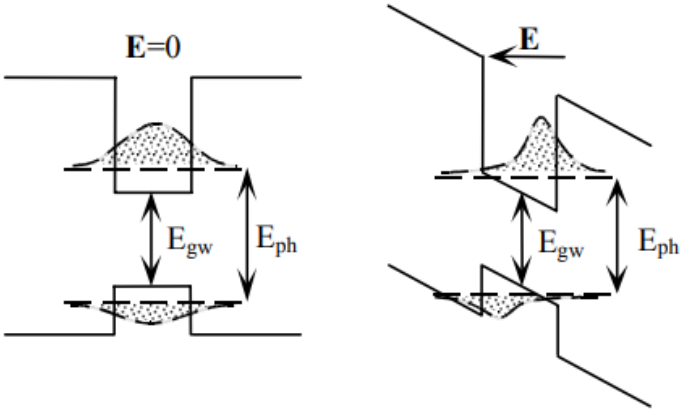


Figure 2.16: Illustration of quantum confined stark effect[35]

Both bulk materials and quantum well materials type modulators offer their advantages. Quantum well materials have higher modulation efficiencies due to lower optical voltage, while bulk materials are less wavelength sensitive, culminating in a larger optical bandwidth [34].

- **Mach-Zehnder Modulator :** This modulator is based on the electro-optic effect, in which the reflective index of a material, usually Lithium Niobate ($LiNbO_3$), changes with the application of different voltages across its electrodes [24]. The $LiNbO_3$ MZM is used instead of other electro-optic modulators because it presents low losses, large extinction ration, low chirp and small wavelenght dependence [37].

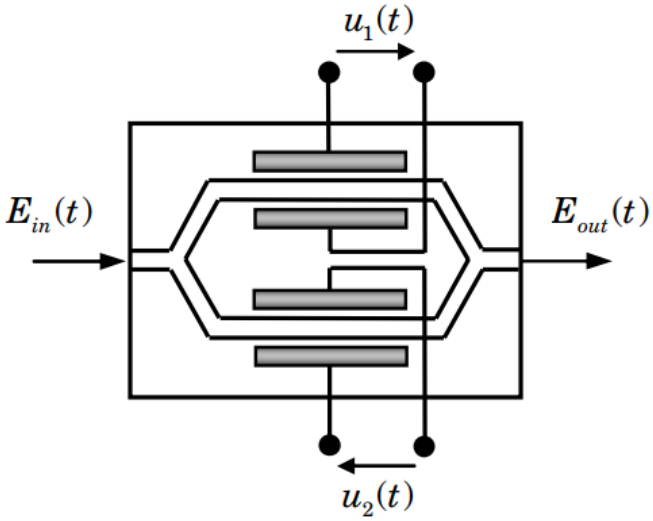


Figure 2.17: Integrated optical Mach-Zehnder modulator[38]

Figure 2.17 shows a simple representation of an MZM. The incoming light passes through a Y-junction where it is divided by an upper and lower arms where $LiNbO_3$ is located. Here, each arm will induce a phase shift and, after passing through another Y-junction, the two optical fields are recombined. Depending on the relative phase shifts, the interference in the output can vary between constructive (relative phase shift 0) and destructive (relative phase shift is pi). Neglecting the insertion loss, the equation 2.9[38] gives the relation between the input and output fields.

$$E_{out}(t) = \frac{1}{2}(e^{j\phi_1(t)} + e^{j\phi_2(t)})E_{in}(t) \tag{2.9}$$

where $\phi_1(t)$ and $\phi_2(t)$ represent the phase shifts in the upper and lower arms, respectively. For a driving voltage $V_{\pi_1}$ and $V_{\pi_2}$ that obtains a phase shift of $\pi$ in the upper and lower arms, respectively, and an applied voltage $u_1(t)$ and $u_2(t)$ (shown in figure 2.17), phase shifts are given by[38]

$$\phi_1(t) = \frac{u_1(t)}{V_{\pi_1}}\pi; \phi_2(t) = \frac{u_2(t)}{V_{\pi_2}}\pi \tag{2.10}$$

If the phase shifts induced in the two arms are identical ($\phi_1(t) = \phi_2(t) = \phi(t)$), for instance, by setting $u_1(t) = u_2(t) = u(t)$ and $V_{\pi_1} = V_{\pi_2} = V_\pi$, the MZM is operating in push-push mode. On the other hand, when $u_1(t) = -u_2(t) = \frac{u(t)}{2}$ and $V_{\pi_1} = V_{\pi_2} = V_\pi$, phase shifts on both arms become symmetrical ($\phi_1(t) = -\phi_2(t)$), causing the MZM to operate in push-pull mode and have a chirp-free amplitude modulation [38]. With this, we can rewrite the equation 2.9 as:

$$E_{out}(t) = cos(\frac{u(t)}{2V_\pi})E_{in}(t) \tag{2.11}$$

By squaring 2.11 the relation between the input and output power can be written as:

$$\frac{P_{out}(t)}{P_{in}(t)} = \frac{1}{2} + \frac{1}{2}cos(\frac{u(t)}{V_\pi}\pi) \tag{2.12}$$

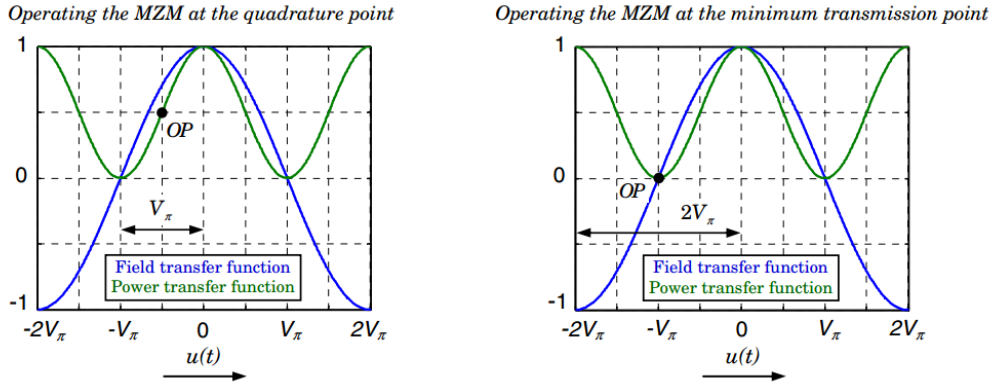


Figure 2.18: Operating the MZM in the quadrature point (a) and the minimum transmission point (b)[38]

Figure 2.18 shows two principles of MZM operation, which are the quadrature (figure 2.18a) and the minimum transmission points (figure 2.18b). For modulation, the MZM is operated at the quadrature point, with a DC bias of $-V_\pi/2$ and a peak-to-peak modulation of $V_\pi$. When operating at the minimum transmission point, with DC bias

of $-V_\pi$ and a peak-to-peak modulation of $2V_\pi$, there is a phase skip of $\pi$ when crossing the minimum transmission point [38].

- **IQ Modulator:** Figure 2.19 illustrates the IQ Modulator. As can be seen, it is composed by two arms (I and Q arm) each having an MZM operating in push-pull mode. The signal is equally divided by the two arms and, after passing through the MZMs, a phase shift of $\pi/2$ is made to one of them. Finally, the signal of both branches is recombined. In this way, it is possible to represent any point of the constellation in the complex IQ-plane [38].

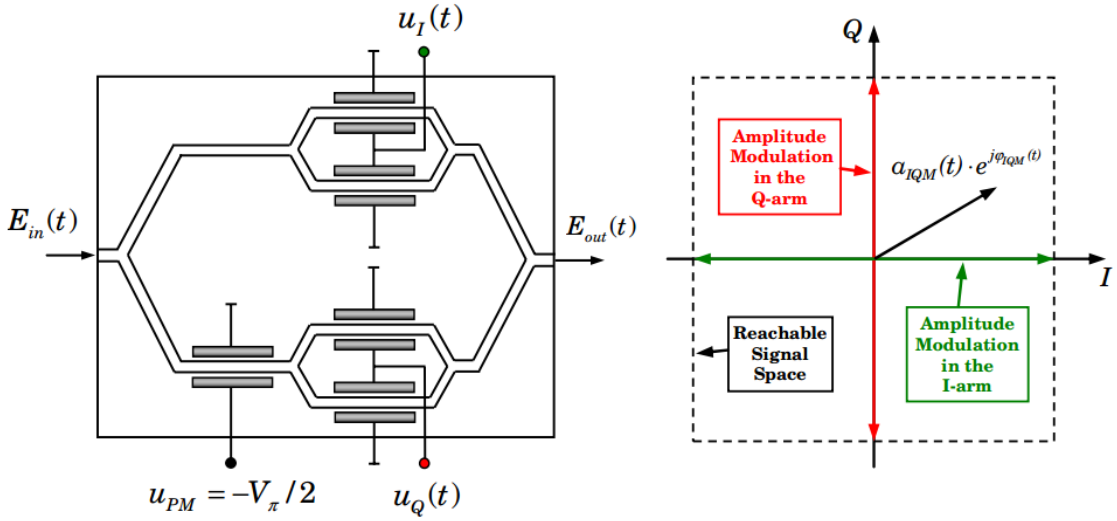


Figure 2.19: Illustration of IQ modulator (a) and Principle of IQ modulation (b) [38]

The output electric field is given by the sum of the two modelated signals after their recombination. Neglecting the insertion loss and consider that the MZMs have the same half wave voltage of $V_\pi$, $E_{out}$ is given by [38]

$$E_{out}(t) = \left[cos\left(\frac{u_I(t)}{2V_\pi}\pi\right) + jcos\left(\frac{u_Q(t)}{2V_\pi}\pi\right)\right]\frac{E_{in}(t)}{2} \tag{2.13}$$

In this way it is possible to verify that the I and Q components of $E_{out}$ are dependent on the MZM driving voltage, being the first dependent on the MZM driving voltage of the upper arm and the second of the lower arm. Since the output electrical signal is a complex number, the amplitude modulation and phase modulation of IQM can be defined as [38]

$$a_{IQM}(t) = \frac{E_{in}(t)}{2}\sqrt{cos^2\left(\frac{u_I(t)}{2V_\pi}\pi\right) + cos^2\left(\frac{u_Q(t)}{2V_\pi}\pi\right)} \tag{2.14}$$

$$\varphi_{IQM}(t) = arg\left[cos\left(\frac{u_I(t)}{2V_\pi}\pi\right), cos\left(\frac{u_Q(t)}{2V_\pi}\pi\right)\right] \tag{2.15}$$

### 2.5.2 Optical receiver

The optical receiver is where the detection and conversion of the signal from optical to electrical takes place, as well as the recover of the transmitted data. One of the most commonly used detection techniques is noncoherent detection, also known as direct detection, which, being the simplest, only allows a recover of information for modulation formats which encode the information in the power of the optical carrier. Another of the most commonly used detection techniques is coherent detection which, being more complex, is used for more advanced modulation formats that encode the information in phase as in the power of the optical carrier. In fact, the main purposes of coherent detection are to linearly recover the I and Q components of the incoming signal, and to suppress or cancel the common mode noise [24].

#### 2.5.2.1 Noncoherent Detection

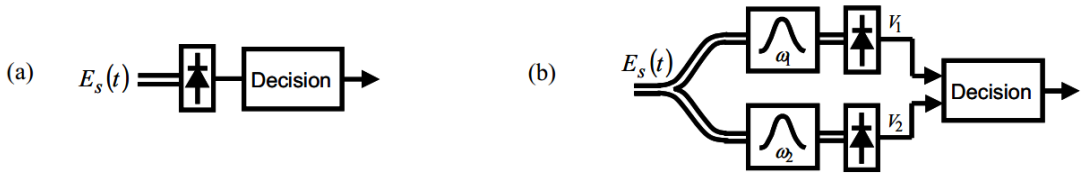


Figure 2.20: Illustration of noncoherent detection for (a) ASK and (b) BFSK[39]

In noncoherent detection, the receiver makes decisions based in the measurement of the energy of the incoming signal. In figure 2.20 we can see an illustration of this detection technique, where is simply implemented with a photodiode. This same principle can be used to collect information from Binary Frequency Shift Keying (BFSK), here being necessary to separate the two frequencies $w_1$ and $w_2$. Noncoherent detection has some drawbacks, such as having only one degree of freedom (DOF) per polarization per carrier, reducing in this way the spectral efficiency and power efficiency. Other disadvantage is the fact that loss of phase information during detection is an irreversible transformation, which prevents full equalization of linear channel impairments like chromatic dispertion (CD) and polarization mode dispertion (PMD) by linear flters. Even when maximum-likelyhood sequence detection (MLSD) is applied, the performance is suboptimal when compared to optical or electrical equalization processes that use the full electric field [39].

#### 2.5.2.2 Coherent Detection

In contrast to direct detection, coherent detection is a synchronous process that requires the use of an local oscillator (LO) obtained through the use of an additional laser. The principle behind coherent detection is the product of the received optical carrier and the continuous-wave LO. The optic signal that comes from the transmitter can be described by [40]

$$E_S(t) = A_S(t)e^{(jw_S t)} \tag{2.16}$$

where $A_S$ represents the complex amplitude and $w_S$ the angular frequency. Likewise, the electric field of LO can be described by

$$E_{LO}(t) = A_{LO}(t)e^{(jw_{LO} t)} \tag{2.17}$$

where $A_{LO}$ and $w_{LO}$ represents the complex amplitude and the angular frequency of LO, respectively. The powers of the optical fields can be described by $P_S = |A_S|^2/2$ and $P_{LO} = |A_{LO}|^2/2$, where $P_S$ is the power of the signal and $P_{LO}$ the power of LO. Note that this last one is always constant.

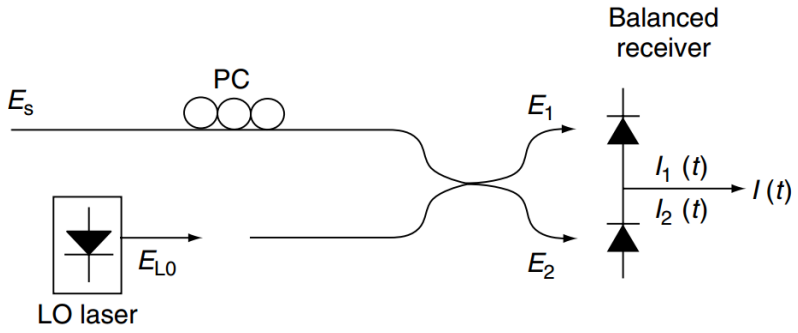


Figure 2.21: Illustration of a coherent detection scheme[40]

In figure 2.21 is shown a coherent detection illustration, where the balanced detection method is employed. This method is used to suppress the DC component and maximize the signal photocurrent. It consists in the use of an optical coupler that adds $180^{\circ}$ phase shift to one of the two optical fields. When the signal and LO are copolarized, the electric field incident on the photodiodes is described by [40]

$$E_1 = \frac{1}{\sqrt{2}}(E_S + E_{LO}) \tag{2.18}$$

$$E_2 = \frac{1}{\sqrt{2}}(E_S - E_{LO}) \tag{2.19}$$

The resulting photocurrents are given by [40]

$$I_1(t) = \frac{R}{2}\left[P_S + P_{LO} + 2\sqrt{P_S P_{LO}}cos(w_{IF}t + \theta_{sig}(t) - \theta_{LO}(t))\right] \tag{2.20}$$

$$I_2(t) = \frac{R}{2}\left[P_S + P_{LO} - 2\sqrt{P_S P_{LO}}cos(w_{IF}t + \theta_{sig}(t) - \theta_{LO}(t))\right] \tag{2.21}$$

where $w_{IF}$ represents the intermediate frequency given by $w_{IF} = w_S - w_{LO}$, $\theta_{sig}(t)$ and $\theta_{LO}(t)$ are the phases of the transmitted and LO, respectively, and R the responsitivity of the photodiode, given by [40]

$$R = \frac{e\eta}{\hbar w_S} \tag{2.22}$$

where $\hbar$ stands for the Planck's constant divided by $2\pi$, $e$ is the electron charge, and $\eta$ is the quantum efficiency of the photodiode. Note that the sum frequency component is discarded because, due to limited bandwidth of the photodiode, it will be averaged out to zero. The balanced detector output is given by [40]

$$I(t) = I_1(t) - I_2(t) = 2R\sqrt{P_S P_{LO}}cos(w_{IF}t + \theta_{sig}(t) - \theta_{LO}(t)) \tag{2.23}$$

Note that $\theta_{sig}$ only includes the phase noise that varies with time [40].

Coherent detection presents several advantages when compared with direct detection. It allows the transmission of information by modulating the amplitude, phase or frequency of the opticl carrier. Direct detection does not allow phase or frequency modulation, since all phase information is lost on transmission. This opens the possibility of using more advanced modulation formats.

#### 2.5.2.3 Homodyne Coherent Detection

In this coherent-detection technique, the frequency of the LO, $w_{LO}$, is such that it coincides with the frequency of the signal $w_s$, making $w_{IF} = 0$. The photocurrent is given by [33]

$$I(t) = R(P_S + P_{LO}) + 2R\sqrt{P_S P_{LO}}cos(\theta_S(t) - \theta_{LO}(t)) \tag{2.24}$$

Usually $P_{LO}$ is much bigger than $P_S$, making $P_S + P_{LO} \approx P_{LO}$. The last term of 2.24 is the part that contains the information, used by the decision circuit. In the case where the local oscillator phase is locked to the signal phase so that $\theta_S = \theta_{LO}$, the homodyne signal is given by [33]

$$I_P(t) = 2R\sqrt{P_S P_{LO}} \tag{2.25}$$

The main advantage of the homodyne detection is shown when we analyze equation 2.25, if we consider that the signal current in the direct detection scheme is given by $I_{dd}(t) = RP_S(t)$. Considering the optical average power by $\bar{P_S}$, the average electrical power is increased by a factor of $4P_{LO}/\bar{P_S}$, with the use of homodyne detection. Homodyne detection also improves the SNR by a large factor, due to the fact that $P_{LO}$ can be much larger than the $P_S$, making power enhancement exceeding 20 dB [33].

A disadvantage of using homodyne detection is its phase sensitivity. The equation 2.24 has, in the last term, the local oscillator phase $\theta_{LO}$ that should be controlled. Ideally $\theta_S$ and $\theta_{LO}$ should be kept constant. In practice, they vary with time on a random way but, with the implementation of an optical phase-locked loop, its difference ($\theta_S$ - $\theta_{LO}$) can be conserved. The implementation of such a loop adds complexity, making the design of optical homodyne detection receivers quite complicated. In addition there is a need for matching the transmitter and LO frequencies placing strict requirements on the two optical sources. [33].

#### 2.5.2.4 Heterodyne Coherent Detection

For heterodyne detection, the LO frequency $w_{LO}$ is chosen such that its difference with the signal carrier frequency $w_0$ results in a intermediate frequency $w_{IF}$ in the microwave region. The photocurrent of this type of detection is given by [33]

$$I(t) = R(P_S + P_{LO}) + 2R\sqrt{P_S P_{LO}}cos(w_{IF}t + \theta_S(t) - \theta_{LO}(t)) \tag{2.26}$$

Because $P_{LO}$ is much larger than $P_S$, the first term of equation 2.26 (corresponding to the DC component of the signal) is practically constant, being easily removed with the use of bandpass filters. We can then rewrite 2.26 only with its AC component, resulting in [33]

$$I_{ac}(t) = 2R\sqrt{P_S P_{LO}}cos(w_{IF}t + \theta_S(t) - \theta_{LO}(t)) \tag{2.27}$$

As in homodyne detection, in this detection scheme LO also amplifies the received signal by a large factor, improving the SNR. However, due to AC nature of $I_{ac}$, the average signal power is reduced in half, making the SNR of heterodyne detection decrease by a factor of 2 (3 dB) when compared to homodyne detection [33].

The design of the heterodyne detection receiver is much simpler than that of the homodyne detection due to the fact that it does not requires the implementation of a phase-locked loop. Narrow-linewidth semiconductor lasers are used for the two optical sources as a way to control both $\theta_S$ and $\theta_{LO}$ variations. The linewidth requirements are quite reasonable for

asynchronous demodulation schemes, making heterodyne detection a very applicable scheme in practical applications of coherent systems [33].

#### 2.5.2.5 Photodetectors

The photodiode is a fundamental part of the receiver, having as role the absorption of photons from the optical signal and convert to electrical signal through the reverse process of what occurred in the laser. The p-i-n photodiode (PIN) and avalanche photodiode (APD) are among the most common types of photodiodes [24].

- **PIN photodiode :** The PIN photodiode consists of a reverse biased p-n junction with a layer of undoped or lightly doped semiconductor material between p- and n-type layers. This layer will increase the depletion region while minimizing the diffusion current component. Due to the almost intrinsic nature of the material, the middle i-layer offers a very high internal impedance making most of the voltage drop occur across it [33]. Due to this internal impedance and to the fact that PIN is reversed biased, it acts as a current source generating a proportional photocurrent to incoming optical signal power [24]. In figure 2.22 we see an illustration of the PIN photodiode.

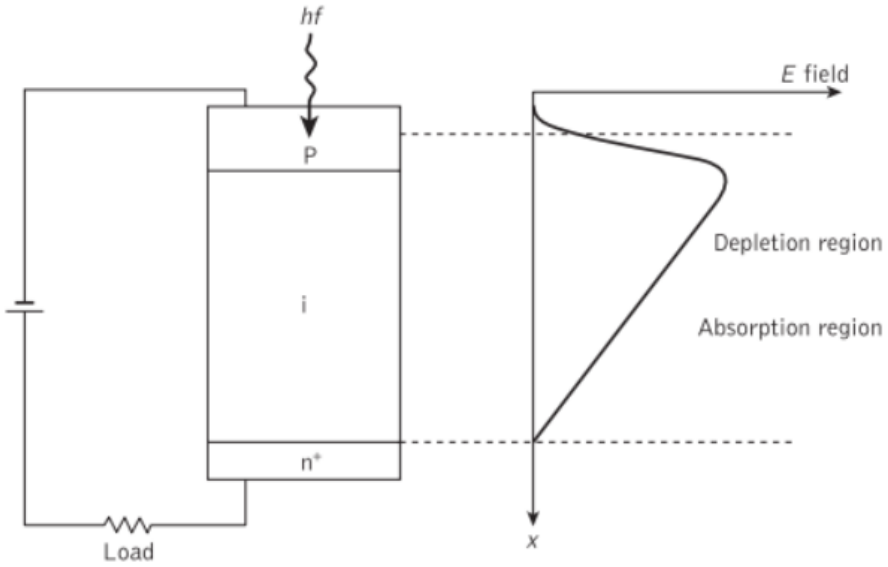


Figure 2.22: PIN photodiode with combined depletion and absorption region [1]

The depletion region, where the absorption of the incident photons takes place, can be controlled by controlling the i-layer width [1]. By increasing its width, the responsiveness will increase and the response time will increase as well, being precise so there is a compression between sensitivity and speed [33].

- **APD photodiode :** An APD is a modified PIN which has an additional p-layer responsible for creating an extremely high electric field region which causes an internal current gain [1], as shown in figure 2.23.

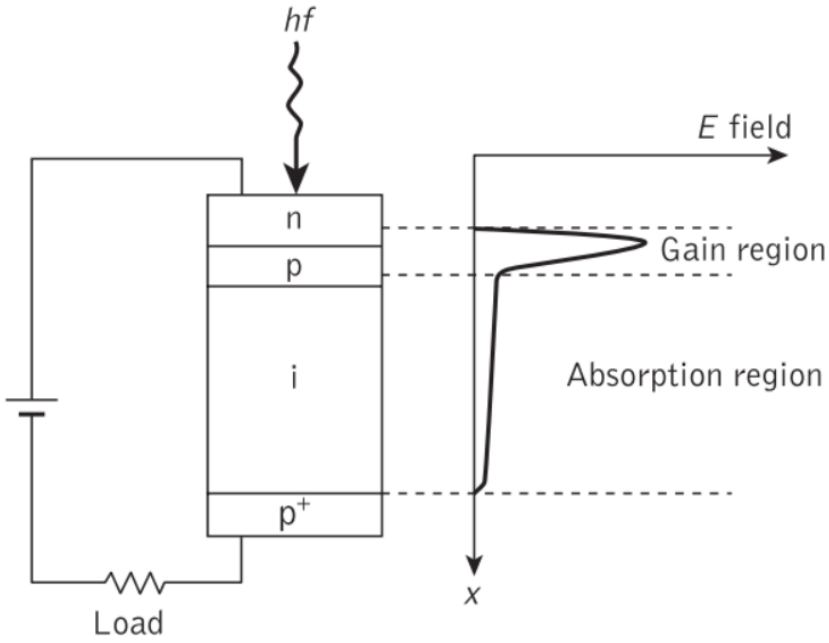


Figure 2.23: APD photodiode ilustration with internal gain and absorption region [1]

The depletion region continues to be where photons are absorbed, just as happens in PIN photodiodes. The difference is in the high field region, where holes and electrons can acquire enough energy to excite new electron-holes pairs. This phenomenon is responsible for the internal current gain and is known as impact ionization [1].

This photodiode has some advantages over photodiodes without internal gain. Usually it has a better sensitivity than PIN photodiodes and, due to its gain variation with reversed bias and response time, has a wider dynamic range [1].

### 2.5.3 Receiver sensivity

The receiver sensivity is very important to understand the impact the transmitted signal suffers on the way to the receiver. It's made with the BER that counts the number of errors in the received signal and EVM that estimates the position of a symbol from the ideal position in the constellation.

#### 2.5.3.1 Error Vector Magnitude

Error vector magnitude (EVM) is a metric performance used on modern communication systems to access the quality of a received signal [41], that is, is the difference between the expected complex voltage of a symbol after the demodulation and the actual value of the received symbol. EVM measures, this way, the quality of the signal when compared to the expected received symbol. Since real systems are always subject to signal degradation factors, such as non-linear effects, dispersion or attenuation, the symbol received will often not be exactly as expected [42].

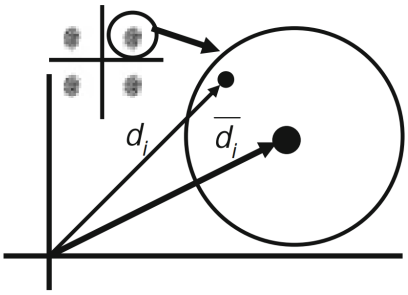


Figure 2.24: Definition of the EVM [24]

Figure 2.24 shows an EVM illustration consisting on amplification of the constellation in which the largest point in the circumference's center represents the theoretical point where the symbol should be located at and the smallest point represents the received symbol. It is possible to calculate EVM through [24]

$$EVM(\%) = 100 * \frac{\overline{\left\|d_i - \overline{d_i}\right\|^2}^{1/2}}{d_{max}} \tag{2.28}$$

where $d_i$ represents the distance between the received symbol and the center of the constellation referential, $\overline{d_i}$ consists of the distance between the expected received symbol and the center of the referential, and $d_{max}$ is the maximum distance that a point can have in relation to the expected received symbol and the center of the constellation.

#### 2.5.3.2 Relationship between EVM and BER

The EVM value can also be mathematically described by [43]

$$EVM_{RMS} = \frac{\frac{1}{N}\sum_{n=1}^{N}|S_n - S_{0,n}|^2}{\frac{1}{N}\sum_{n=1}^{N}|S_{0,n}|^2} \tag{2.29}$$

where $S_n$ is the normalized nth symbol in the stream of measured symbols, $S_{0,n}$ is the ideal normalized constellation point of the nth symbol and N is the number of unique symbols in the constellation[43]. With this it is possible to BER from EVM, where BER is an aproximation of [44]:

$$BER \approx \frac{2(1-\frac{1}{L})}{log_2 L} Q\left[\sqrt{\left[\frac{3log_2 L}{L^2-1}\right]\frac{2}{EVM_{RMS}^2 log_2 M}}\right] \tag{2.30}$$

where L is the number of signal levels identical within each constellation dimension and $log_2 M$ as the number of bits encoded into each symbol. The following figure 2.25 shows the relation between EVM and BER.

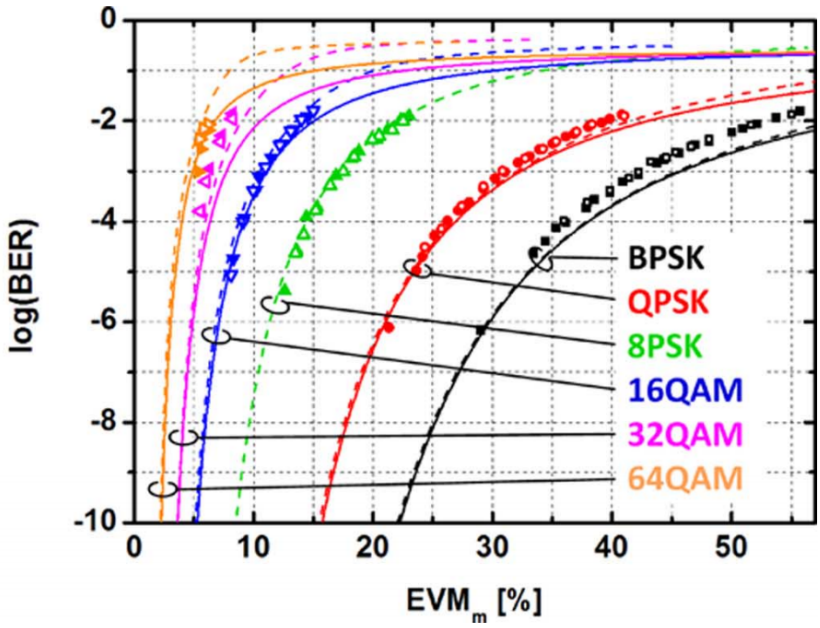


Figure 2.25: Relation between BER and EVM: Measured (symbols), simulated (dashed lines), and calculated BER [44]

# Chapter 3

# Simulation

The simulation was developed using Optisystem software. This software, developed by Optiwave, is widely used by the community for research in the field of Optical Communications. This software enables users to plan, test and simulate optical links in the transmission layer of optical networks. It has several visualizers, both in the optical and electrical domain, as well as a large number of tools that make this software one of the most used for these applications.

Optisystem also have a library of several examples available for various applications and a set of example classes that are very useful and easy to understand. In order to carry out this work, I began by using one of the existing OFDM examples that I have modified according to my needs in order to achieve the desired result.

## 3.1 Simulation setup

The simulation setup of the CO-OFDM system is shown in figure 3.1. Two modulation formats were used, QPSK and 16QAM. As explained in the previous chapter, an OFDM system requires the use of several blocks that can be concatenated in five functional blocks: OFDM transmitter, RF to optical up-converter, optical link, optical to RF down-converter and OFDM receiver. To implement this system in the Optisystem, first is generated a sequence of bits using a sequence generator which is mapped to the desired modulation format (in this case QPSK or 16QAM). IFFT operation was performed in order to get digital time domain signal. It was used 128-points IFFT having 80 subcarriers and a guard interval of 1/8 the symbol window. To remove distortion in the electrical signals, the OFDM signals go by low-pass filters with cut-off frequency of 0.75 symbol rate and depth 100 dB.

After this phase, the signals enter the RF to optical up-converter block (shown with more detail in figure 3.2) where they go by an IQ Modulator. Here is used a CW laser diode along with two MZM modulators to map I and Q of RF OFDM signal onto an optical carrier. It should be noted that the CW laser diode operates with a central frequency of 193.1 THz and the linewidth is set to 0.1 MHz. After 90° phase change by one of the signals, the two signals are then recombined and transmitted through the optical channel.

The optical channel consists of SSMF in which the length is varied for each test. The optical fiber was set to have a dispersion coefficient of 17 ps/nm/km, dispertion slope of 0.075 ps/nm$^2$/Km, PMD coefficient of 0.05 ps/sqrt(km) and attenuation of 0.2 dB/Km. After the optical channel, it is used a Goussian filter to remove the Goussian optical noise on the optical

OFDM signal.

In the optical to RF down-converter, the optical coherent receiver block was used to detect the optical signal on the receiver side. Is in this block that is located both the photodetector (PIN or APD) and the LO. The LO was set to have a constant power of 10 dBm. It also converts the optical signal into an electrical signal. Then, an OFDM demodulator is used to recover the original signal.

A bit rate of 40 Gbit/s was used which induces a symbol rate of 20 GBd for the case of QPSK and 10 GBd for 16QAM (due to the use of 2 and 4 bits per symbol, respectively). It was used a sequence length of $2^{15}$ bits in this simulations.

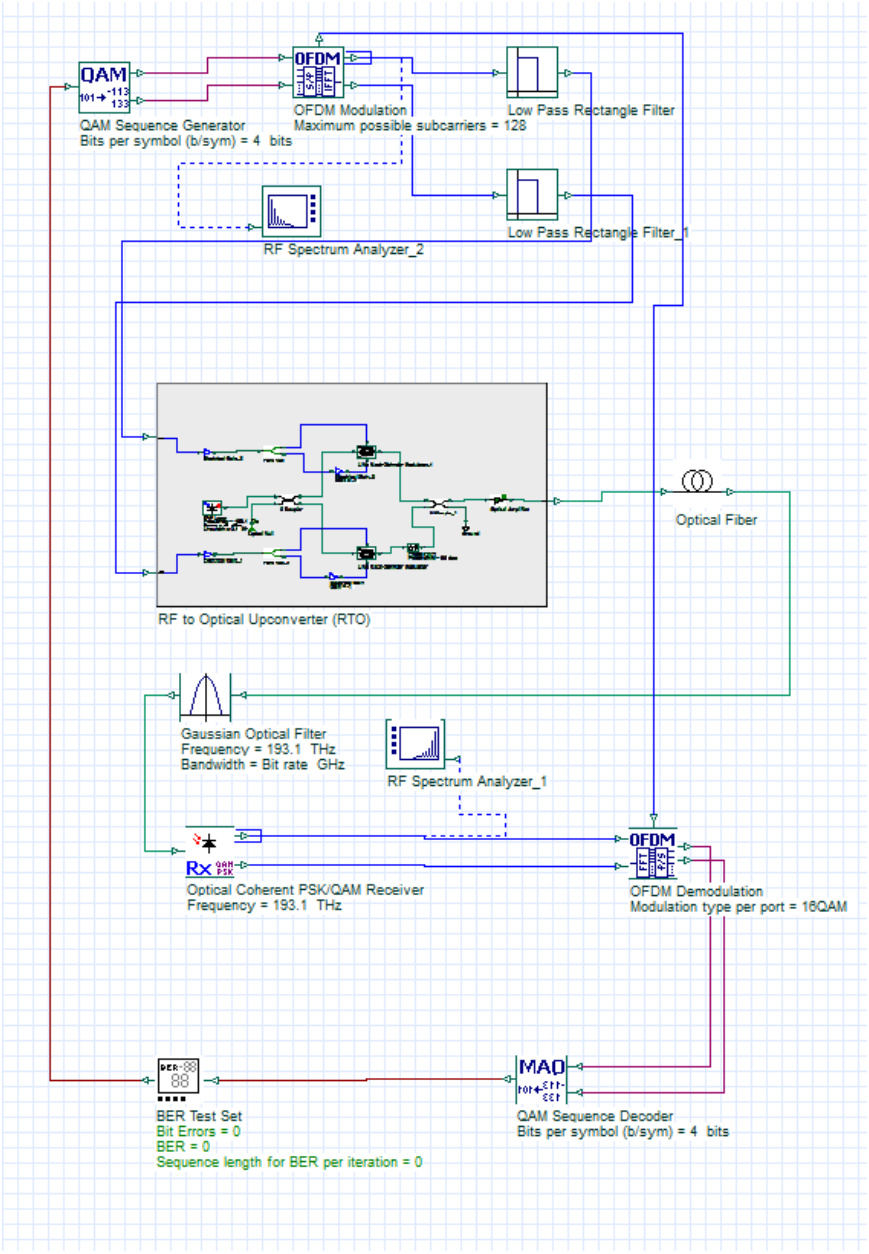


Figure 3.1: Coherent detection simulation setup

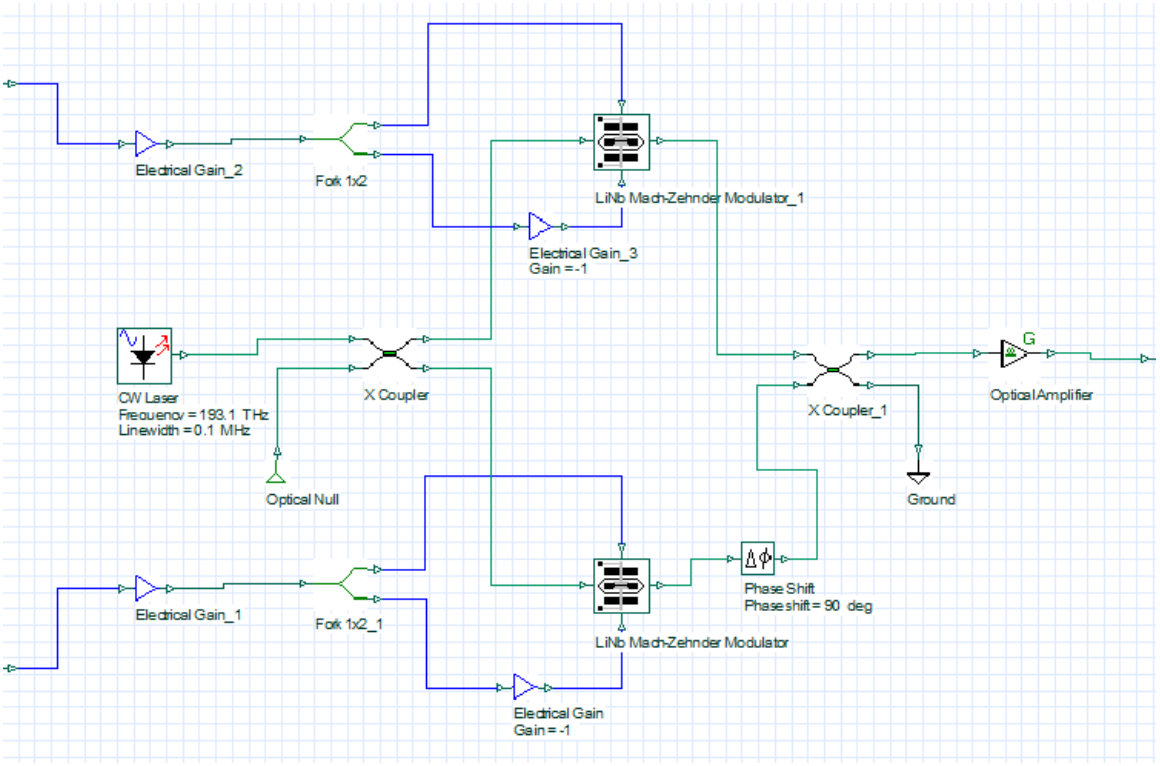


Figure 3.2: RF to Optical up-converter subsystem

Figure 3.3 shows the setup used for direct detection simulation. The main difference between the two simulation setups used is, in addition to the type of detection, the type of modulator used, being IQ modulator for the case of coherent detection and Intensity Modulator in the form of MZM for direct detection.

Like coherent detection, this setup uses a sequence generator to generate a pseudo random bit sequence which is then mapped to the desired modulation format. The mapped symbols then pass through the OFDM modulator where it's converted from serial to parallel. The Quadrature Modulator then modulates I and Q components separately and sends it to the MZM modulator where, along with a CW laser diode, maps I and Q of RF OFDM onto an optical carrier. After this phase, the signal is sent to the optical link which has the same characteristics as that used in the simulation of coherent detection. The signal passes through a Gaussian optical filter and reaches the receiver. The receiver consists of a photodetector (PIN or APD) tuned at the same frequency as the CW laser diode. The converted electrical signal then passes through the Quadrature Demodulator and an OFDM demodulator with the same specifications as the OFDM modulator. Finally, the signal passes through a sequence decoder that maps the symbols back to bits, that are used for BER analysis. The BER measurement is done in the BER test set block.

All settings such as bit rate, sequence length, IFFT points, number of subcarriers and guard interval were maintained between coherent detection and direct detection since one of the goals was to see how the different types of detection reflect on the results.

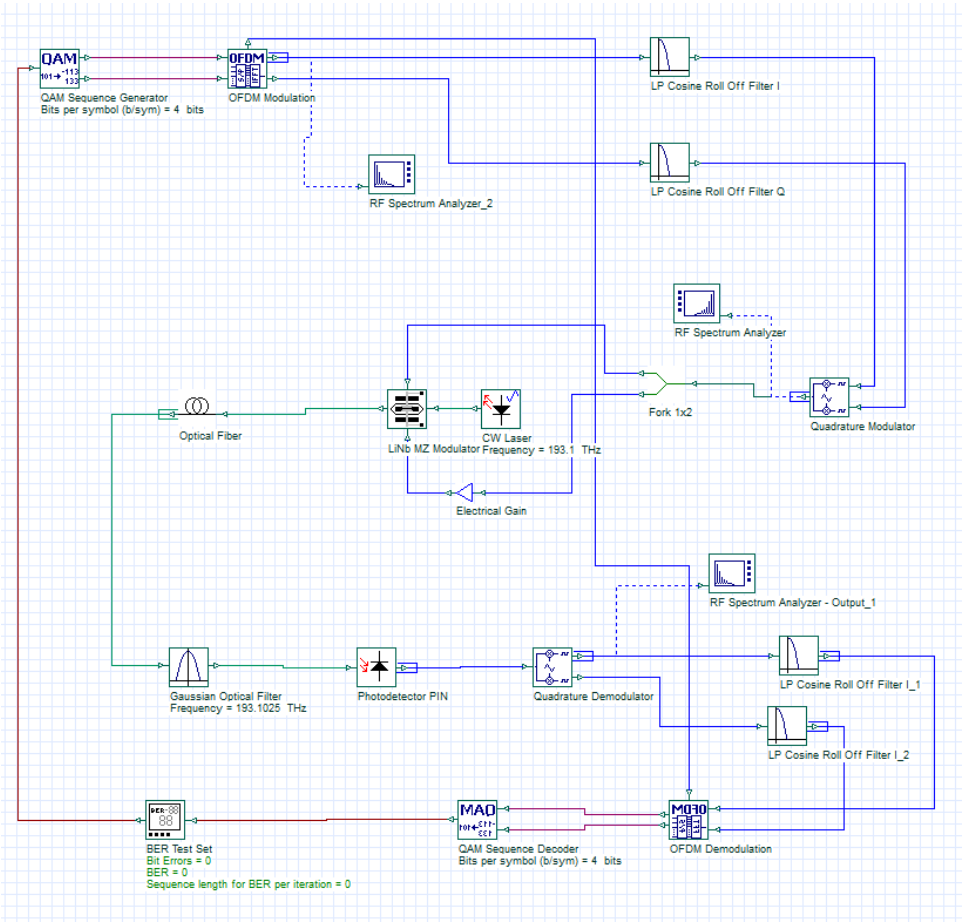


Figure 3.3: Direct detection simulation setup

Table 3.1: Fiber specifications

| **Parameter** | **Value** |
|---|---|
| Dispersion | 17 ps/nm/km |
| Attenuation | 0.2 dB/km |
| Effective area | 80 um^2 |

## 3.2 Simulation results and analysis

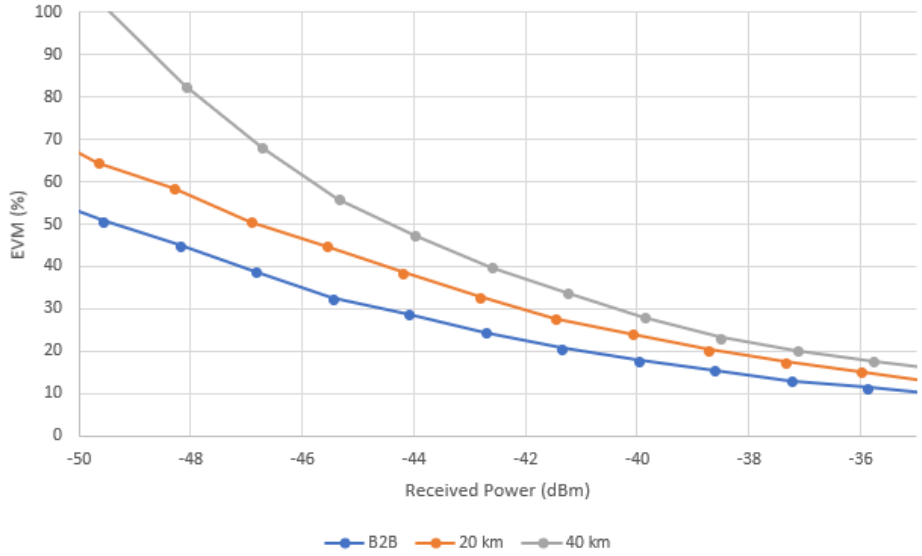


Figure 3.4: QPSK results of EVM VS Received power using Coherent Detection

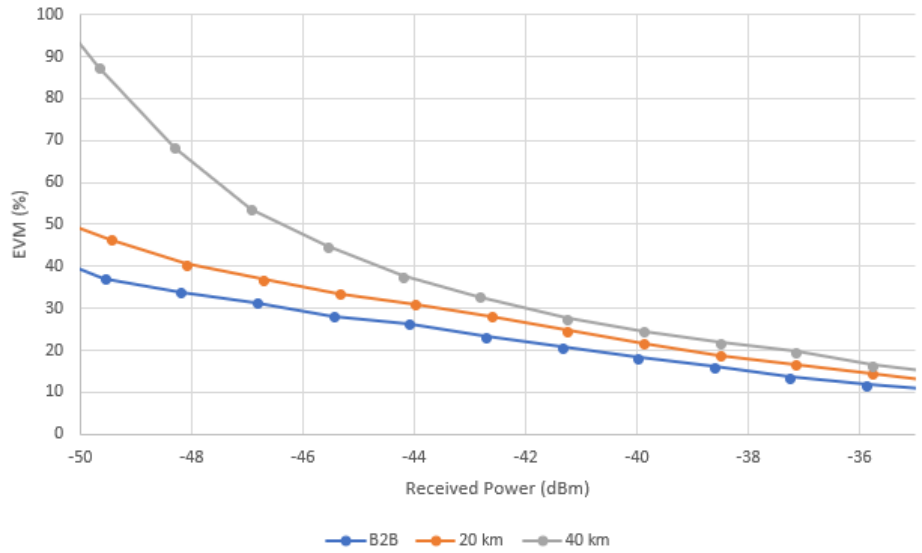


Figure 3.5: 16QAM results of EVM VS Received power using Coherent Detection

Figures 3.4 and 3.5 show the dependence of EVM with received power for coherent detection, both using PIN photodiode. As seen in 2.5.3.1, EVM is a measure of signal quality that compares the received signal with the expected signal. Comparing the two figures it's possible to see that, for the same received power, QPSK has an EVM value higher than 16QAM.

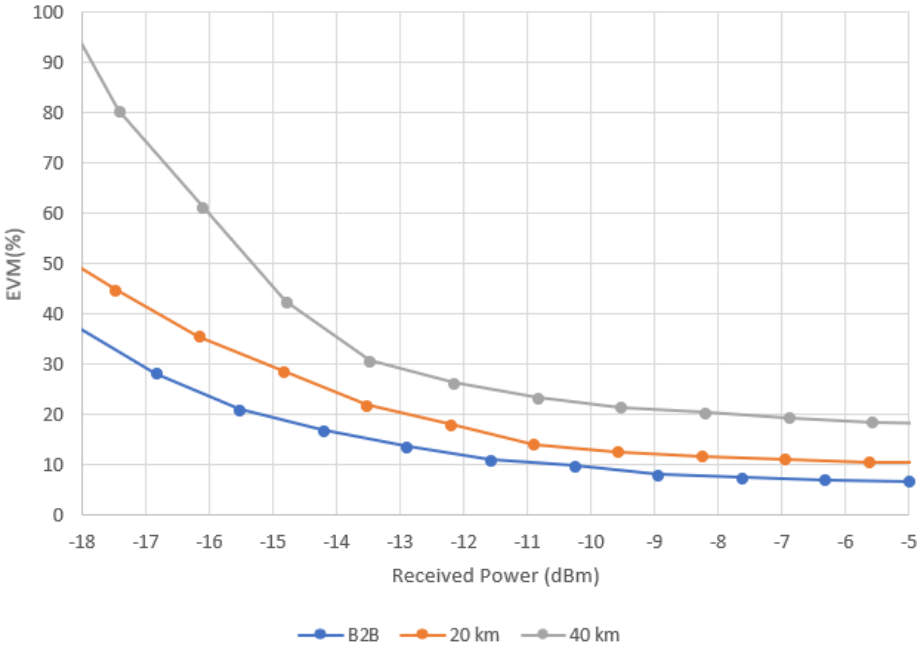


Figure 3.6: QPSK results of EVM VS Received power using Direct Detection

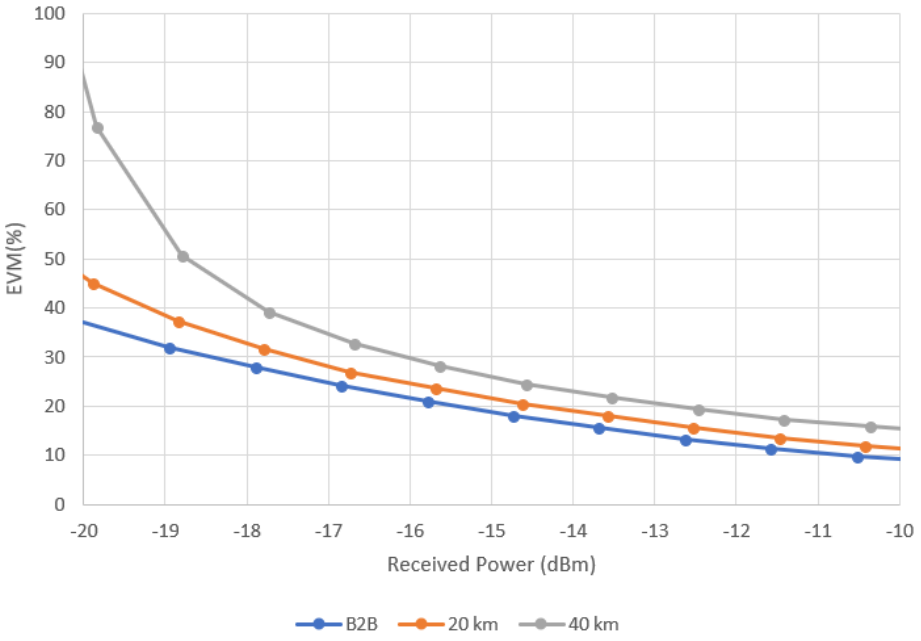


Figure 3.7: 16QAM results of EVM VS Received power using Direct Detection

In figures 3.6 and 3.7, where direct detection was used, the obtained results were similar to those of coherent detection, where the QPSK modulation obtained higher EVM values than 16QAM.

Due to the number of bits per symbol and the transmission rate used for this simulation,

QPSK has a symbol rate of 20 GBd while 16QAM has a symbol rate of 10 GBd, making the QPSK bandwidth two times bigger than the one of 16QAM, which has a higher spectral efficiency. Since QPSK has 2 bits per symbol while 16QAM has 4 bits per symbol, an error in one of the QPSK bits will have a greater implication in the result than an error on one bit in a symbol having 4 bits per symbol provoking an increase in EVM and explaining the differences obtained between QPSK and 16QAM.

In order to obtain the results of log(BER) versus Transmitted Power, the CW laser diode was set in sweep mode where the power started at -55 dBm and increased until log(BER) passes the value of -3. This value is considered as an approximation of the value of FEC [45], this being the value from which the BER is such that it allows the recovery of the transmitted signal. For each iteration, the log(BER) was measured with the aid of BER Test Set block. This procedure was repeated for several fiber lengths and all parameters were kept the same in all tests, varying only the length of the optical link.

On the receiver side, it is possible to change the photoreceptor between PIN and APD simply by changing its block, for the case of direct detection. In the case of coherent detection, this procedure has to be done in the Coherent Receiver block, where LO is also found.

Figure 3.8 and 3.9 show the evolution of the BER for different lengths of optical fiber using the PIN receiver and coherent detection, varying the modulation format between QPSK and 16QAM.

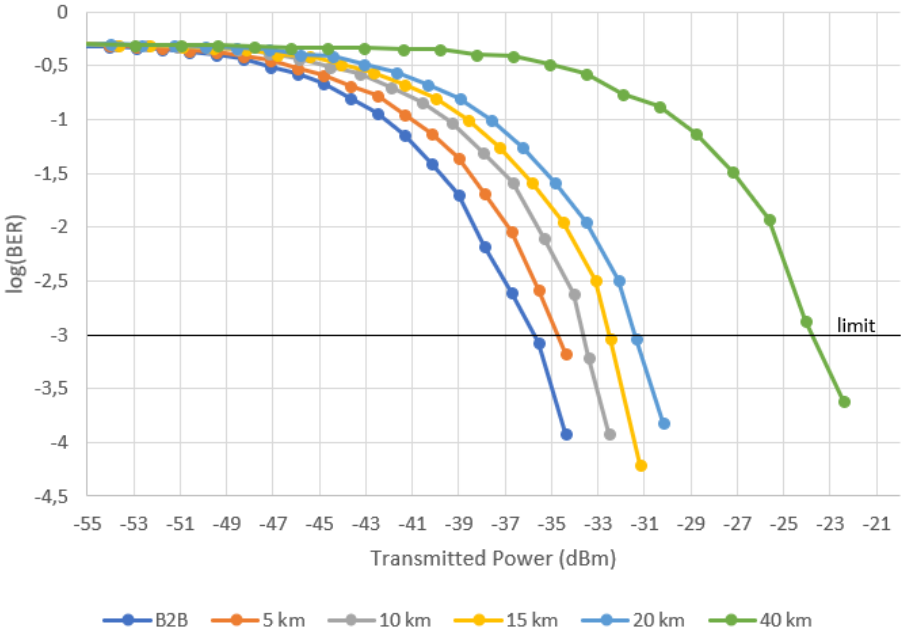


Figure 3.8: QPSK results of log(BER) VS Transmitted power using PIN receiver and Coherent Detection

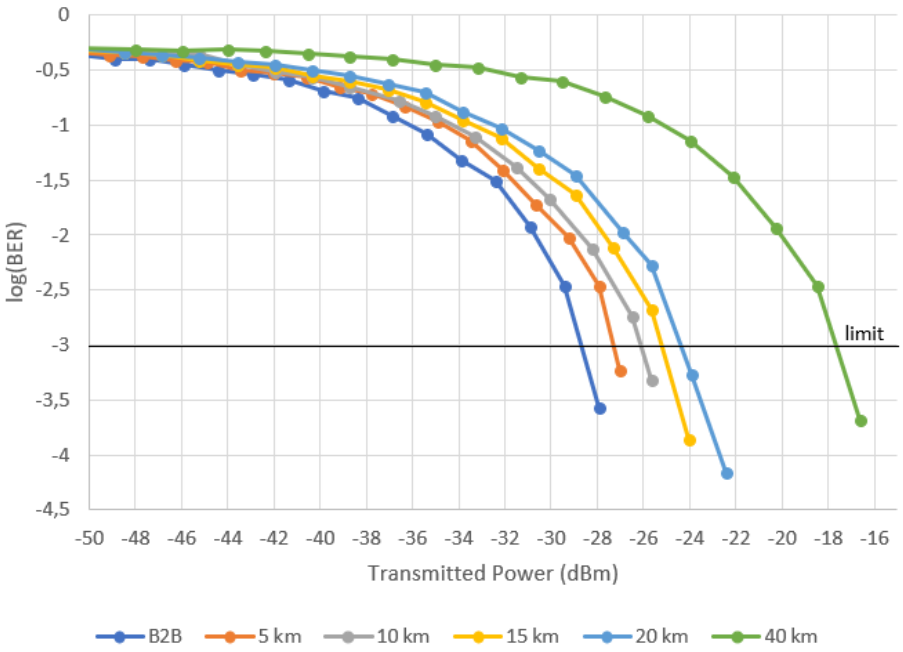


Figure 3.9: 16QAM results of log(BER) VS Transmitted power using PIN receiver and Coherent Detection

In figure 3.8 it is possible to conclude that the sensitivity of the receiver is -36 dBm for B2B with a near linear evolution per each 5 km of fiber added (for fiber lenghts of 5, 10 and 15 km) of about 1.1 dB. Since the specification of the optical link used has an attenuation of 0.2 dB / km, it will cause an increase of 1 dB in the receiver per 5 km of additional optical fiber, where the other penalties can be caused by nonlinear effects and chromatic diespersion. There is a sensitivity of -31.5 dBm for 20 km and, for 40 km, it is -23.8 dBm. In figure 3.9 we see that the sensitivity of the receiver is about -28.8 dBm for B2B and, as for figure 3.8, there is an increase of about 1 dB per 5 km of fiber added to the receiver (for fiber lenghts of 5, 10 and 15 km) that can also be justified with fiber attenuation, nonlinear effects and chromatic dispersion. For 20 and 40 km, the measured sensivity is -24.5 dBm and -17.7 dBm, respectively. Comparing the two modulation formats, we see that the sensitivity of 16QAM greater. This is due to the higher required OSNR for 16QAM.

Figure 3.10 and 3.11 show the evolution of the BER for different lengths of optical fiber using an APD receiver and coherent detection, varying between QPSK and 16 QAM.

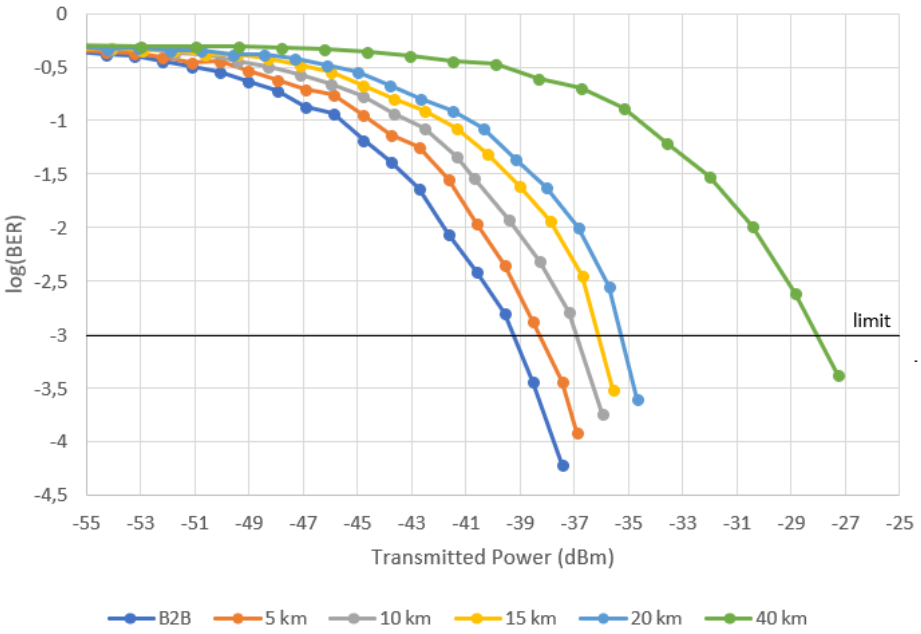


Figure 3.10: QPSK results of log(BER) VS Transmitted power using APD receiver and Coherent Detection

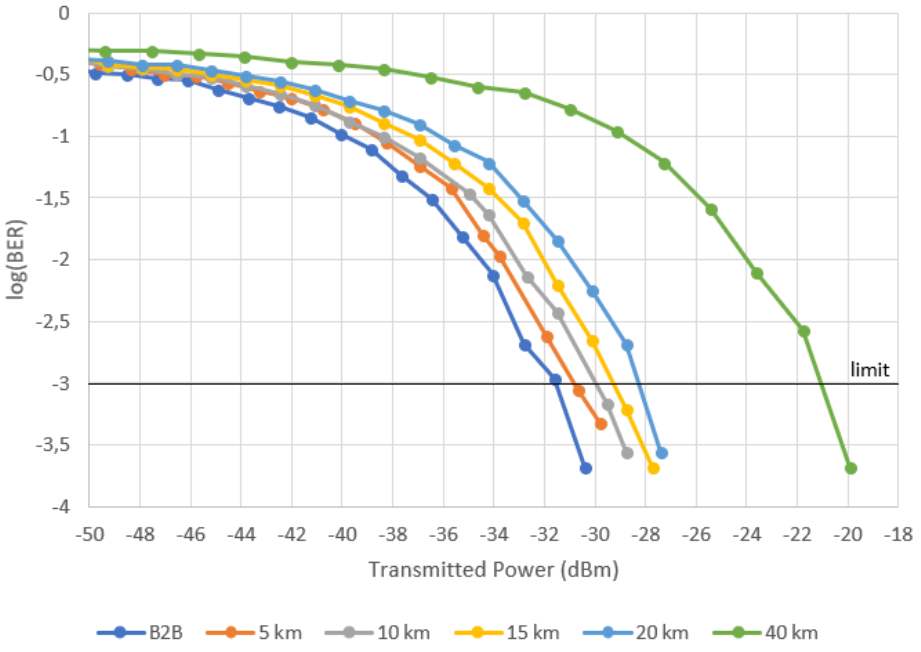


Figure 3.11: 16QAM results of log(BER) VS Transmitted power using APD receiver and Coherent Detection

In figure 3.10 we can see that the sensitivity of APD photodiode for QPSK is about -39.1 dBm for B2B and that, similar to what happens for the PIN photodiode, there is an increase

of about 1 dB per 5 km of optical fiber added to the optical link (for shorter distances of 5, 10 and 15 km). For 20 km the sensitivity is -35.2 dBm and, for 40 km, is -28.1 dBm. In figure 3.11 we see that the sensitivity of the receiver is about -31.7 dBm for B2B and also with an increase of about 1 dB per 5 km of fiber added due to the effect of attenuation inherent in the optical fiber. The sensitivity for 20 km is -28.3 dBm while, for 40 km, is -21.1 dBm. The difference in sensitivity between the two modulation formats is about 7.4 dB for B2B being the highest sensitivity referring to the 16QAM modulation format which can also be explained by the distance between symbols of this modulation format being smaller when compared to QPSK. Comparing the two receptor types we see that the photoreceptor APD sensitivity is higher than PIN. This result is expected because APD has an internal gain.

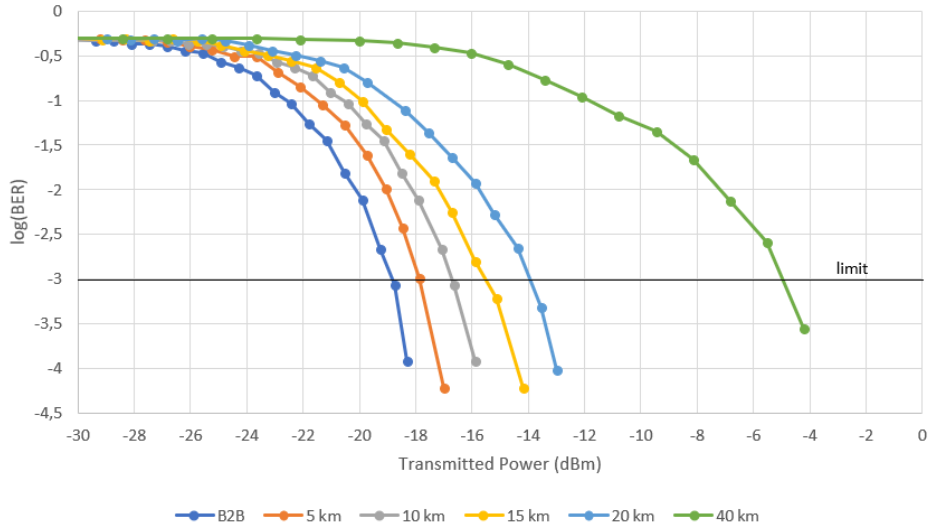


Figure 3.12: QPSK results of log(BER) VS Transmitted power using PIN receiver and Direct Detection

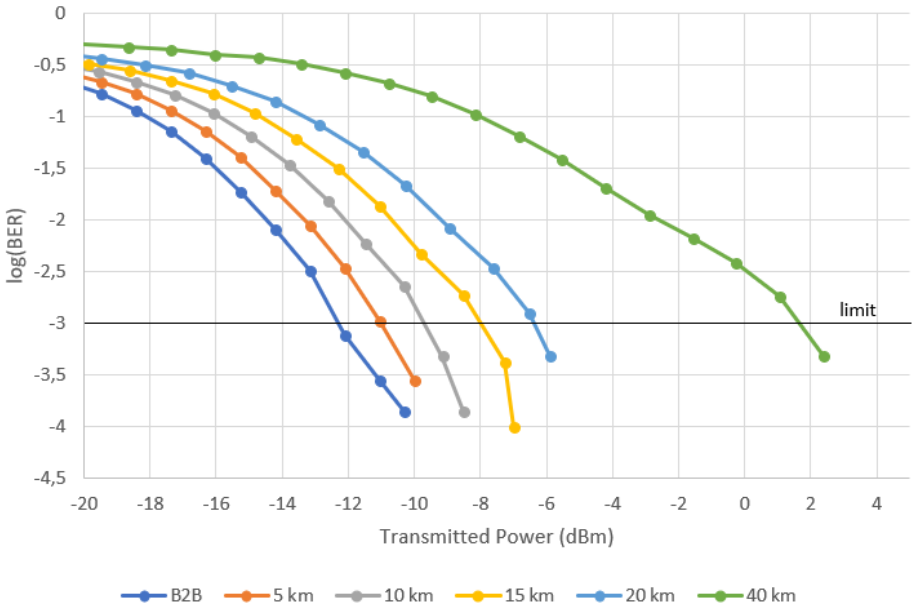


Figure 3.13: 16QAM results of log(BER) VS Transmitted power using PIN receiver and Direct Detection

It can be seen in figure 3.12 that the sensitivity of the PIN photodiode to this setup using direct detection is -18.8 dBm for B2B with an increase of about 1dB per 5 km of fiber added to the optical link (for 5, 10, 15 km). for 20 km there is a sensitivity of -13.9 dBm and, for 40 km, -5 dBm. In the case of 16QAM (figure 3.13), the corresponding sensitivity of B2B is -12.4 dBm, with an increase higher than in the case of QPSK for distances of 5, 10 and 15 km. The recorded sensitivity for 20 and 40 km was -6.4 and 1.7 dBm, respectively. It is possible to see that the latter setup (figure 3.13) is more susceptible to factors like non-linear effects and chromatic dispersion than the setup used for QPSK, since the losses are larger.

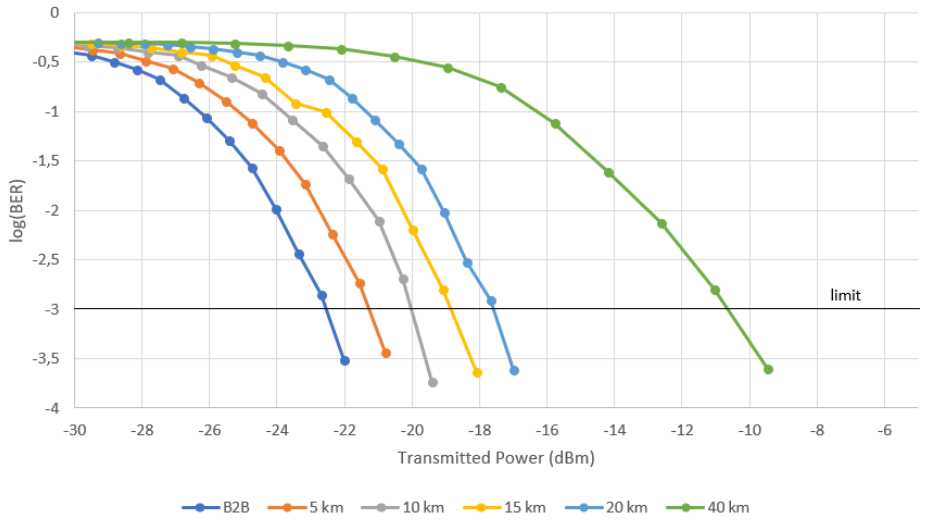


Figure 3.14: QPSK results of log(BER) VS Transmitted power using APD receiver and Direct Detection

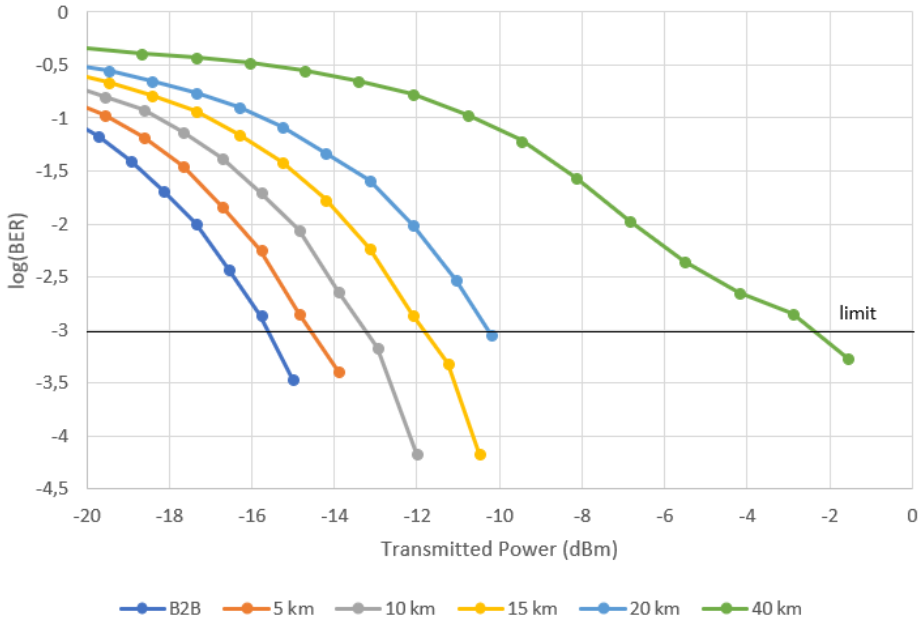


Figure 3.15: 16QAM results of log(BER) VS Transmitted power using APD receiver and Direct Detection

For QPSK (figure 3.14) we can see that the sensitivity of APD phododiode for B2B is -22.6 dBm with an increase of about 1.2 dB with the increase of every 5 km of fiber (for fiber distances of 5, 10 and 15 km). For 20 km it is -17.6 dBm and, for 40 km, it is -10.7 dBm. In the case of 16QAM (figure 3.15), the sensitivity for B2B is -15.7 dBm and here, similar to what happens with the PIN photodiode, there is a greater increase for distances of 5, 10 and 15 km than for QPSK. A sensitivity of -10.3 dBm was measured for 20 km and, for 40 km,

-2.5 dBm. It is noticeable a much higher received power when comparing coherent detection with direct detection. Since coherent detection uses a local oscillator (essentially a second laser), it will inject extra power in the system.

In order to plot the results of log(BER) versus Received Power an attenuator was placed after the optical link. Having a constant power from the CW laser diode applied to the fiber and having the attenuator in sweep mode, the received power was measured and, in the BER test set block, the value of log(BER) was also measured for each iteration. The maximum and minimum value of the attenuator was adjusted so that it results on a log(BER) that passes the value of -3 for each optical link length, thus allowing to plot the log(BER) versus Received Power.

On the receiver side, like for the case of log(BER) versus Transmitted Power, the photoreceptor can be changed between PIN and APD simply by changing the block or in the the Optical Coherent Receiver block, for the case of direct detection and coherent detection, respectively.

When measuring the received power we are removing the effect of fiber attenuation on the system and only considering the effect of chromatic dispersion and nonlinear effects. This way it is possible to analyze the response of each system directly to these phenomena.

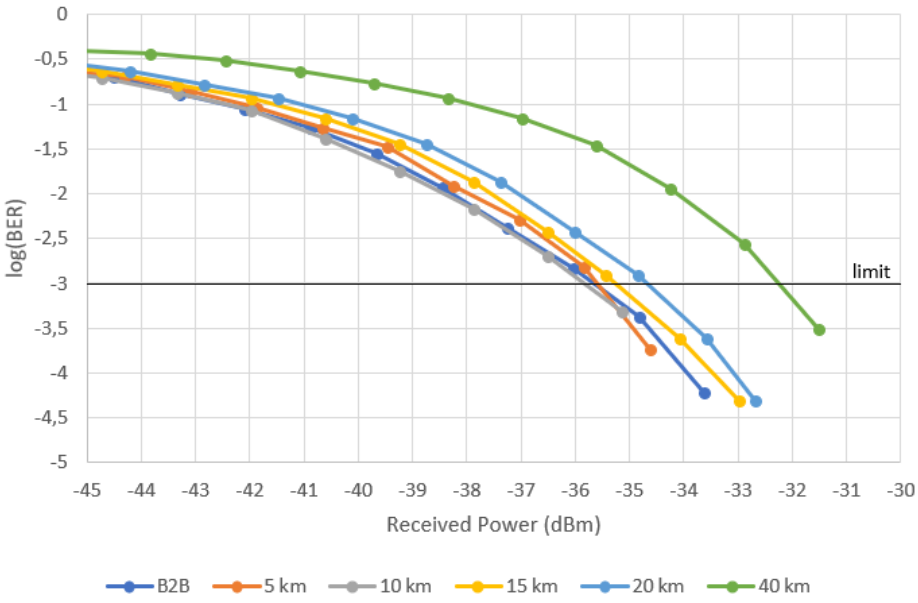


Figure 3.16: QPSK results of log(BER) VS Received power using PIN receiver and Coherent Detection

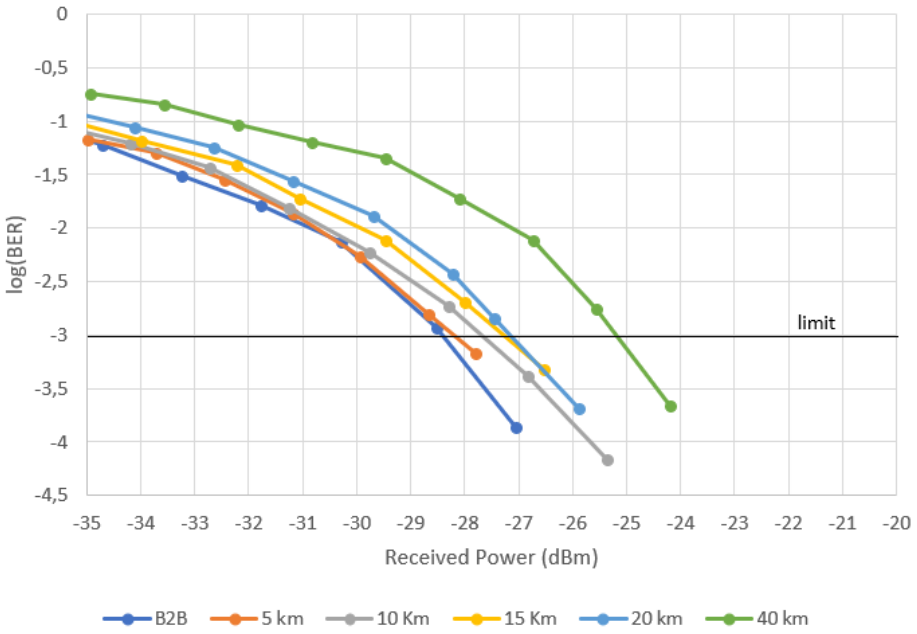


Figure 3.17: 16QAM results of log(BER) VS Received power using PIN receiver and Coherent Detection

In figure 3.16 and 3.17 we can see the results of log(BER) versus Received power for QPSK and 16QAM, both for photoreceptor PIN and Coherent Detection. We can see that for QPSK we have a sensitivity of -35.7 dBm for B2B, with results for 5, 10 and 15 km with deviations of about 0.6 dB while, for 20 and 40 km we have -34.7 dBm and -32.3 dBm, respectively. For this case there is a difference of 1 dB between B2B and 20 km and of 3.4 dB between B2B and 40 km, which is caused by dispersion and non-linear effects.

For 16QAM we have a sensitivity of -28.5 dBm for B2B, with a higher power variation received for shorter fiber distances of 1.2 dB for 5, 10 and 15 km than for the case of QPSK. For 20 km we have a received power of -27.2 dBm (which is 1.3 dB higher when compared with B2B) while for 40 km it is -25.3 dBm (3.2 dB higher than B2B).

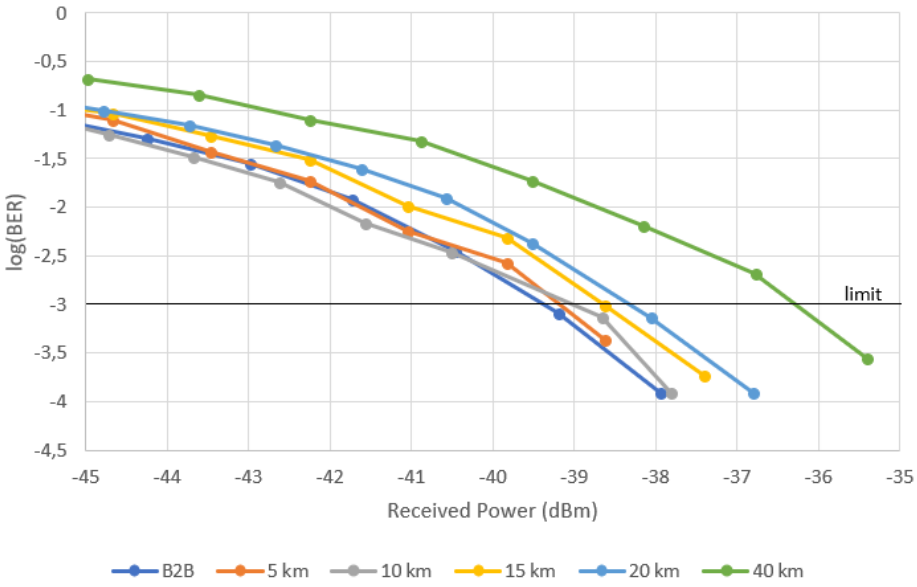


Figure 3.18: QPSK results of log(BER) VS Received power using APD receiver and Coherent Detection

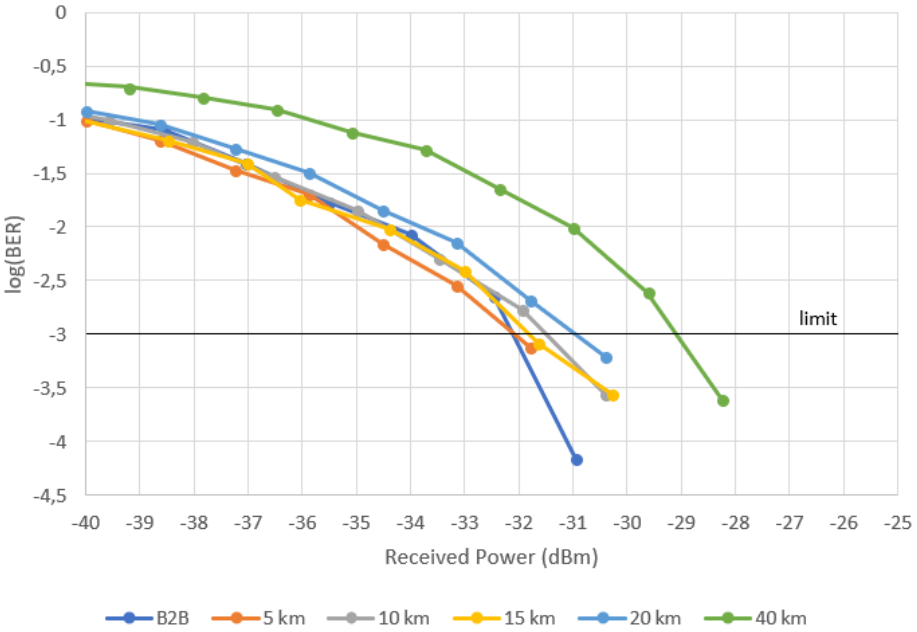


Figure 3.19: 16QAM results of log(BER) VS Received power using APD receiver and Coherent Detection

In figure 3.18 and 3.19 we have the results of log (BER) versus Received Power using APD photoreceptor and coherent detection. For QPSK we have a sensitivity of -39.4 dBm for B2B, with a variation of 0.7 dB for smaller distances of 5, 10 and 15 km, -38.4 dBm for 20 km and

-36.3 dBm for 40 km, with a penalty of 1 dB and 3.1 dB for 20 km and 40 km, respectively, when compared to the sensitivity recorded for B2B.

For 16QAM there is a sensitivity of -32.1 dBm for B2B, with a smaller deviation of 0.3 dB for smaller distances of 5, 10 and 15 km, -31.1 dBm for 20 km and -29.1 dBm for 40 km. In this case we have a penalty of 1.1 dB and 3 dB for 20 km and 40 km, respectively, when compared to the sensitivity of B2B.

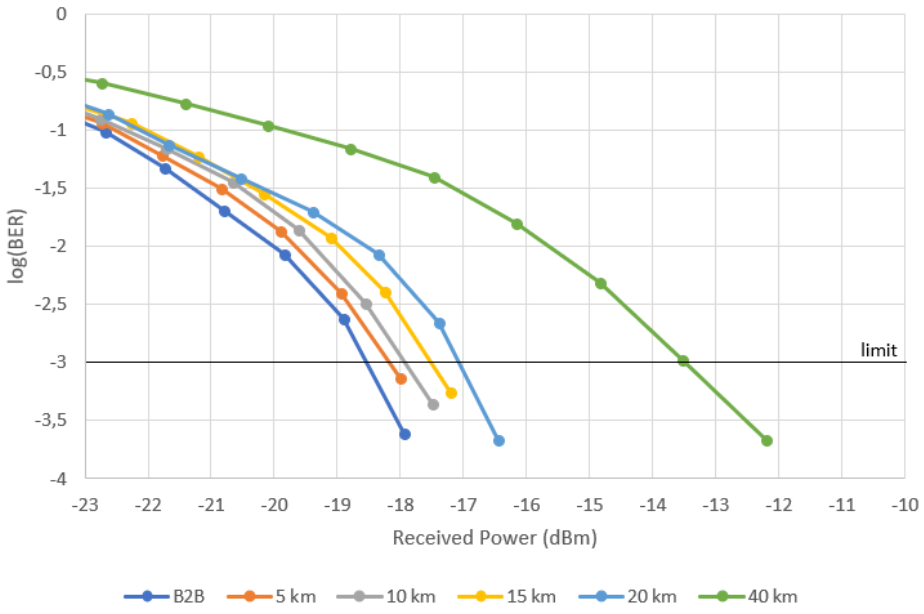


Figure 3.20: QPSK results of log(BER) VS Received power using PIN receiver and Direct Detection

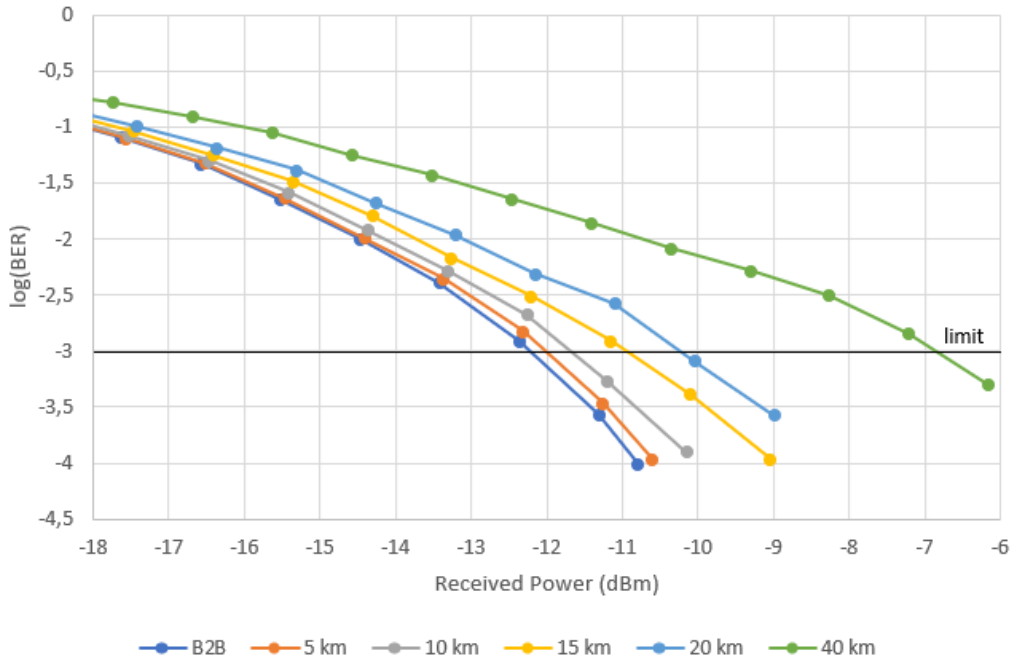


Figure 3.21: 16QAM results of log(BER) VS Received power using PIN receiver and Direct Detection

In figures 3.20 and 3.21 it is possible to see the simulation results for log(BER) versus received power using direct detection and PIN with QPSK for the first and 16QAM for the second. The sensitivity of QPSK for B2B is -18.6 dBm, 20 km has a penalty of 1.5 dB with a received power for this distance of -17.1 dBm and, for 40 km, a penalty of 5 dB when compared with B2B, with a received power of -13.6 dBm.

16QAM has a higher sensitivity and suffers more penalties than QPSK. The measured sensitivity for B2B is -12.3 dBm, for 20 km is -10.3 dBm with a 2 dB penalty and, for 40 km, is measured a sensitivity of -6.9 dBm with, in this case, a penalty of 5.3 dB.

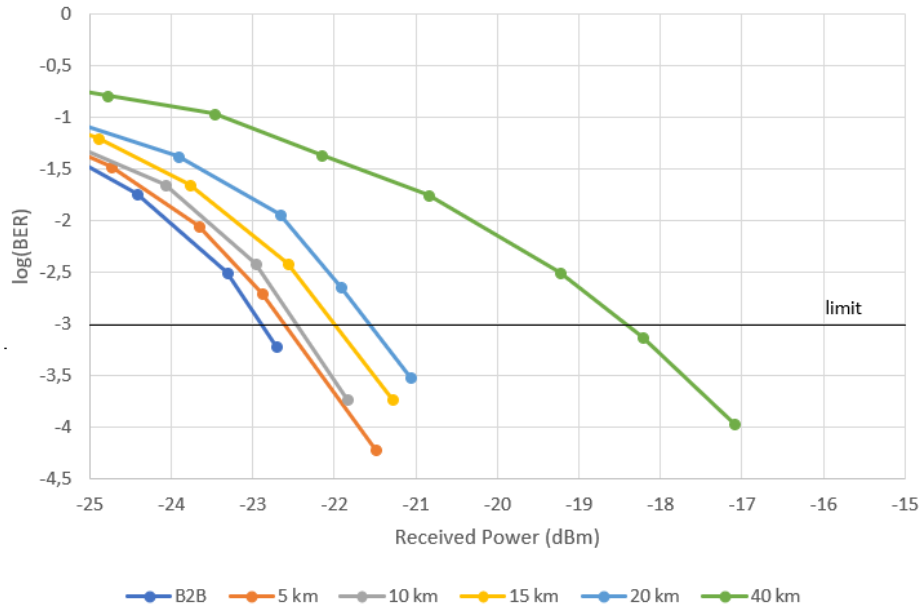


Figure 3.22: QPSK results of log(BER) VS Received power using APD receiver and Direct Detection

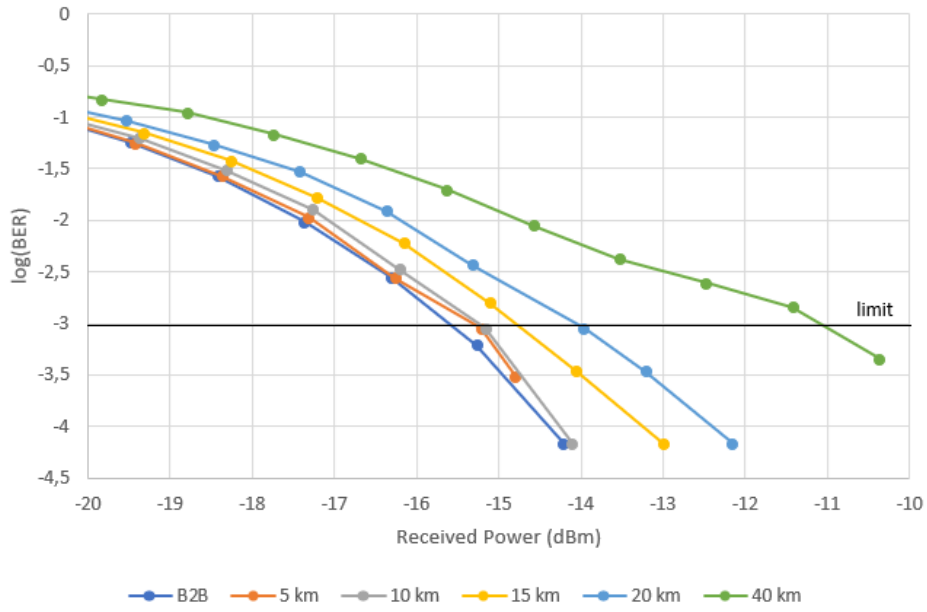


Figure 3.23: 16QAM results of log(BER) VS Received power using APD receiver and Direct Detection

In figure 3.22 it is possible to see that the sensitivity of APD photodiode for QPSK is -22.8 dBm for B2B and that there is a power increase of 1.2 dB for the 20 km, the sensitivity of which is -21.6 dBm. For the case of 40 km, a sensitivity of -18.4 dBm is measured, the penalty being 4.4 dB when compared to B2B. For 16QAM, figure 3.23, a sensitivity of -15.6

dBm is measured for B2B. 20 km has a penalty of 1.5 dB, with a sensitivity of -14.1 dBm and, for 40 km, 4.4 dB, the latter having a sensitivity of -11.2 dBm.

[10]

Table 3.2: B2B, 20 km and 40 km simulation results for log(BER) versus Received Power

| | | | **QPSK** | **16QAM** |
|---|---|---|---|---|
| **PIN** | **IM-DD** | B2B | -18.6 dBm | -12.3 dBm |
| | | 20 km | -17.1 dBm | -10.3 dBm |
| | | 40 km | -13.6 dBm | -6.9 dBm |
| | **IQ-CD** | B2B | -35.7 dBm | -28.5 dBm |
| | | 20 km | -34.7 dBm | -27.2 dBm |
| | | 40 km | -32.3 dBm | -25.2 dBm |
| **APD** | **IM-DD** | B2B | -22.8 dBm | -15.6 dBm |
| | | 20 km | -21.6 dBm | -14.1 dBm |
| | | 40 km | -18.4 dBm | -11.2 dBm |
| | **IQ-CD** | B2B | -39.4 dBm | -32.1 dBm |
| | | 20 km | -38.4 dBm | -31 dBm |
| | | 40 km | -36.3 dBm | -29.1 dBm |

Table 3.2 shows a summary of the results obtained for the different log (BER) versus Received Power. Using this setup in which we always inject the same power on the fiber and an attenuator after the optical link, we are removing the fiber attenuation, only having chromatic dispersion where the optical phase of the signal depends on its wavelength and non-linear effects, which will have a negative effect on the received power.

Analyzing the differences between PIN and APD, we can verify that APD has a better sensitivity in all tests performed. This improvement is justified by the fact that this photoreceptor has an internal gain.

It is quite clear that IQ-modulation coherent detection (IQ-CD) has a much better sensitivity than intensity modulation direct detection (IM-DD) since the former takes advantage by using a local oscillator which injects an extra power. It is also verified on all tests that

direct detection has a greater penalty than coherent detection.

Comparing QPSK with 16QAM we see that 16QAM has, on all simulations performed, a higher received power than QPSK. This penalty is due to the fact 16QAM requires a higher OSNR than QPSK.

It is also possible to see that QPSK has a lower penalty than 16QAM (for the distances tested) so it can be conclude that the latter is more susceptible to nonlinearities.

# Chapter 4

# Conclusions and Future Work

## 4.1 Conclusions

Nowadays there is an increasing need to transfer large amounts of data, requiring the maximum of the current access networks and bringing its' capacity to the limit of their capabilities.

With the constant need to have ever growing bit rates, it is known that optical communications are the only communication technology currently existing that allows bit rates in the order of Terabits. With the standard NG-PON2 is possible to provide 40 Gb/s downstream and 10 Gb/s upstream and there are constant advances in the optical communications field which shows that we are still far from the possible limit of fiber's transmission capacity.

In this master's thesis it was proposed and demonstrated that OFDM-PON is an important technology with advantages in some applications that has to be taken into account for future optical access network.

This thesis was initiated with an introduction to PON technologies, as well as the evolution and requirements that each PON technology demands. Were also given some of the OFDM advantages.

In chapter 2 is given first an overview of some of the most relevant OFDM competing technologies,TDM-PON, WDM-PON, TWDM-PON, as well as their operating principles and the needs that triggered its development. It's also made an extensive theoretical and mathematical study of the generation of an OFDM signal going through all the steps involved in both the electrical and optical part. Lastly was made a study of the two types of detection, direct and coherent, as well as OFDM signal detection and the different photoreceptors used.

In chapter 3, Optiwave Optisystem software was used in all simulations. Two modulation formats were tested, QPSK and 16QAM, as well as two different types of receivers, PIN and APD. Two types of detection were also analyzed, coherent detection and direct detection, the first one being used together with IQ-Modulator made from two MZMs while the second was used together with intensity modulation made with one MZM. Several graphs of the dependence of BER by transmitted power were taken, as well as the dependency of BER and EVM by received power. With this it was possible to draw some conclusions: APD presents better sensitivity for the two modulation formats and for the two types of detection due to the internal gain of the APD; Coherent detection presents a better sensivity than direct detection as well as a minor penalty due to the fact that it has a local oscillator that injects extra power into the system; 16QAM has a higher received optical power than QPSK due to the higher

OSNR required for 16QAM; 16QAM also has higher penalties than QPSK being less tolerant to noise and non-linear effects; regarding EVM, QPSK has worse results than 16QAM due to the higher bandwidth, being less spectral efficient and the impact that a wrong bit has on a two-bit symbol being greater than the impact that a wrong bit has on a four-bit symbol.

## 4.2 Future work

In this master's thesis, all simulations were performed using a bit rate of 40 Gb/s, external modulation with direct and coherent detection. With the constant evolution of the demands requirements from the networks, several solutions must be tested in order to improve the transmission performance. With this, the following topics are proposed as future work:

- Experimental analysis of the results obtained in the simulations.
- Theoretical and experimental analysis of a WDM-OFDM-PON system, the impact that each channel has on the neighboring channel and with different distances between the various channels.
- Theoretical and experimental study of a TWDM-PON system, this being the technology adopted as the standard for NG-PON2, with the same parameters used on this work.

# Bibliography


[1] John M. Senior and M. Yousif Jamro. *Optical Fiber Communications: Principles and Practice*. Pearson Education, 3rd edition, 2009.

[2] Kun Qiu, Xinwen Yi, Jing Zhang, Hongbo Zhang, Mingliang Deng, and Chongfu Zhang. Ofdm-pon optical fiber access technologies. *Communications and Photonics Conference and Exhibition, 2011*, pages 1–9, 2011.

[3] Jun ichi Kani, Fabrice Bourgart, Anna Cui, Albert Rafel, Malcolm Campbell, Russell Davey, and Silvana Rodrigues. Next-generation pon-part i- technology roadmap and general requirements. *IEEE Communications Magazine*, pages 43–49, November 2009.

[4] Shweta Jain, Frank Effenberger, Andrea Szabo, Zhishan Feng, Albert Forcucci, Wei Guo, Yuanqiu Luo, Robert Mapes, Yixin Zhang, and Vincent O'Byrne. World's first xg-pon field trial. *JOURNAL OF LIGHTWAVE TECHNOLOGY*, 29(4):524–528, February 2011.

[5] Xg-pon or xgs-pon: don't make a costly spelling mistake. `https://www.nokia.com/en_int/blog/xg-pon-or-xgs-pon-dont-make-costly-spelling-mistake`. Accessed: 2018-07-03.

[6] Jean Armstrong. Ofdm for optical communications. *Journal of Lightwave Technology*, 27(3):189–204, February 2009.

[7] Nirwan Ansari and Jingjing Zhang. *Media Access Control and Resource Allocation: For Next Generation Passive Optical Networks*. Springer Science and Business Media, 2013.

[8] Leonid G Kazovsky, Ning Cheng, Wei-Tao Shaw, David Gutierrez, and Shing-Wa Wong. *Broadband Optical Access Networks*. John Wiley and Sons, 2011.

[9] Fiber optical networking. `http://http://www.fiber-optical-networking.com/tag/gpon`. Accessed: 2017-10-05.

[10] Amitabha Banerjee, Youngil Park, Frederick Clarke, Huan Song, Sunhee Yang, Glen Kramer, Kwangjoon Kim, and Biswanath Mukherjee. Wavelength-division-multiplexed passive optical network (wdm-pon) technologies for broadband access: a review [invited]. *JOURNAL OF OPTICAL NETWORKING*, 4(11):737–758, November 2005.

[11] Yuanqiu Luo, Xiaoping Zhou, Frank Effenberger, Xuejin Yan, Guikai Peng, Yinbo Qian, and Yiran Ma. Time - and wavelength-division multiplexed passive optical network (twdm-pon) for next-generation pon stage 2 (ng-pon2). *Journal of Lightwave Technology*, 31(4):587–593, February 2013.

[12] Y. Ma, Y. Qian, G. Peng, X. Zhou, X. Wang, J. Yu, Y. Luo, X. Yan, and F. Effenberger. Demonstration of a 40gb/s time and wavelength division multiplexed passive optical network prototype system. In *OFC/NFOEC*, pages 1–3, March 2012.

[13] Xiaofeng Hu, Liang Zhang, Pan Cao, Kongtao Wang, and Yikai Su. Energy-efficient wdm-ofdm-pon employing shared ofdm modulation modules in optical line terminal. *Optical Express*, 20(7):8071–8077, March 2012.

[14] Salem Bindhaiq, Abu Sahmah M. Supa'at, Nadiatulhuda Zulkifli, Abu Bakar Mohammad, Redhwan Q. Shaddad, Mohamed A. Elmagzoub, and Ahmad Faisal. Recent development on time and wavelength-division multiplexed passive optical network (twdm-pon) for next-generation passive optical network stage 2 (ng-pon2). *Optical Switching and Networking*, 15(Supplement C):53 – 66, 2015.

[15] H. Debrégeas, R. Borkowski, R. Bonk, R. Brenot, J. G. Provost, S. Barbet, and T. Pfeiffer. Twdm-pon burst mode lasers with reduced thermal frequency shift. *Journal of Lightwave Technology*, 36(1):128–134, Jan 2018.

[16] S. Dutta, D. Roy, C. Bhar, and G. Das. Online scheduling protocol design for energy-efficient twdm-olt. *IEEE/OSA Journal of Optical Communications and Networking*, 10(3):260–271, March 2018.

[17] W. Shieh, Q. Yang, and Y. Ma. 107 gb/s coherent optical ofdm transmission over 1000-km ssmf fiber using orthogonal band multiplexing. *Opt. Express*, 16(9):6378–6386, Apr 2008.

[18] N. Cvijetic. Ofdm for next-generation optical access networks. *Journal of Lightwave Technology*, 30(4):384–398, Feb 2012.

[19] A. Sano, E. Yamada, H. Masuda, E. Yamazaki, T. Kobayashi, E. Yoshida, Y. Miyamoto, R. Kudo, K. Ishihara, and Y. Takatori. No-guard-interval coherent optical ofdm for 100-gb/s long-haul wdm transmission. *Journal of Lightwave Technology*, 27(16):3705–3713, Aug 2009.

[20] Neda Cvijetic, Ming-Fang Huang, Ezra Ip, Yue-Kai Huang, Dayou Qian, and Ting Wang. 1.2 tb/s symmetric wdm-ofdma-pon over 90km straight ssmf and 1:32 passive split with digitally-selective onus and coherent receiver olt. In *Optical Fiber Communication Conference/National Fiber Optic Engineers Conference 2011*, page PDPD7. Optical Society of America, 2011.

[21] N. Cvijetic, D. Qian, J. Hu, and T. Wang. Orthogonal frequency division multiple access pon (ofdma-pon) for colorless upstream transmission beyond 10 gb/s. *IEEE Journal on Selected Areas in Communications*, 28(6):781–790, Aug 2010.

[22] N. LaSorte, W. J. Barnes, and H. H. Refai. The history of orthogonal frequency division multiplexing. In *IEEE GLOBECOM 2008 - 2008 IEEE Global Telecommunications Conference*, pages 1–5, Nov 2008.

[23] Louis Litwin and Michael Pugel. The principles of ofdm. *RF Signal Processing*, pages 30–48, January 2001.

[24] William Shieh and Ivan Djordjevic. *OFDM for Optical Communications*. Academic Press, 2010.

[25] Ramjee Prasad. *OFDM for Wireless Communications Systems*. Artech House, 2004.

[26] Peng Tan and Norman C. Beaulieu. Reduced ici in ofdm systems using the better than raised-cosine pulse. *IEEE COMMUNICATIONS LETTERS*, 8(3):135–137, March 2004.

[27] S. D. Assimonis, M. Matthaiou, G. K. Karagiannidis, and J. A. Nossek. Optimized better than raised-cosine pulse for reduced ici in ofdm systems. In *2010 17th International Conference on Telecommunications*, pages 249–252, April 2010.

[28] P. Xiao, C. Toal, D. Burns, V. Fusco, and C. Cowan. Transmit and receive filter design for ofdm based wlan systems. In *2010 International Conference on Wireless Communications Signal Processing (WCSP)*, pages 1–4, Oct 2010.

[29] Y. Tang, W. Shieh, X. Yi, and R. Evans. Optimum design for rf-to-optical up-converter in coherent optical ofdm systems. *IEEE Photonics Technology Letters*, 19(7):483–485, April 2007.

[30] Christophe Peucheret. Direct and external modulation of light. *Lecture notes, Department of Photonics Engineering, Technical University of Denmark*, November 2009.

[31] M. Cvijetic. *Optical Transmission Systems Engineering*. Artech House optoelectronics library. Artech House, 2004.

[32] I. Djordjevic, W. Ryan, and B. Vasic. *Coding for Optical Channels*. Springer US, 2010.

[33] Govind P. Agrawal. *Fiber-Optic Communication Systems*. John Wiley and Sons, 3rd edition, 2002.

[34] Joachim Piprek, Yi-Jen Chiu, and John E. Bowers. Analysis of multi-quantum well electroabsorption modulators.

[35] Shengzhong Zhang. *Traveling-wave Electroabsorption Modulators*. PhD thesis, University of California, 1999.

[36] Hans Zappe. *Fundamentals of Micro-Optics*. Cambridge University Press, 2010.

[37] Nazmi A Mohammed, Yasmine El-Guindy, and Moustafa Aly. System optimization to eliminate chirping in dual drive linbo 3 mzm at 40 gb/s. *International Journal of Advanced Engineering Research and Science*, 1:38–46, 07 2014.

[38] M. Seimetz. *High-Order Modulation for Optical Fiber Transmission*. Springer Series in Optical Sciences. Springer Berlin Heidelberg, 2009.

[39] Ezra Ip, Alan Pak Tao Lau, Daniel J. F. Barros, and Joseph M. Kahn. Coherent detection in optical fiber systems. *Optics Express*, 16(2):753–791, January 2008.

[40] Ivan P. Kaminow, Tingye Li, and Alan E. Willner. *Optical Fiber Telecommunications V B: Systems and Networks*. Elsevier Inc., 2008.

[41] T. L. Jensen and T. Larsen. Robust computation of error vector magnitude for wireless standards. *IEEE Transactions on Communications*, 61(2):648–657, February 2013.

[42] Rishad Ahmed Shafik, Md. Shahriar Rahman, AHM Razibul Islam, and Nabil Shovon Ashraf. On the error vector magnitude as a performance metric and comparative analysis. *IEEE–ICET*, pages 27–31, 2006.

[43] R. A. Shafik, M. S. Rahman, A. R. Islam, and N. S. Ashraf. On the error vector magnitude as a performance metric and comparative analysis. In *2006 International Conference on Emerging Technologies*, pages 27–31, Nov 2006.

[44] R. Schmogrow, B. Nebendahl, M. Winter, A. Josten, D. Hillerkuss, S. Koenig, J. Meyer, M. Dreschmann, M. Huebner, C. Koos, J. Becker, W. Freude, and J. Leuthold. Error vector magnitude as a performance measure for advanced modulation formats. *IEEE Photonics Technology Letters*, 24(1):61–63, Jan 2012.

[45] F. Chang, K. Onohara, and T. Mizuochi. Forward error correction for 100 g transport networks. *IEEE Communications Magazine*, 48(3):S48–S55, March 2010.